# Signal extraction from SiPM traces taken by prototype electronics developed for AugerPrime

von

**Jan Paul Koschinsky**

**Bachelorarbeit in Physik**

vorgelegt der
Fakultät für Mathematik, Informatik und Naturwissenschaften
der
Rheinisch-Westfälischen Technischen Hochschule Aachen

**im September 2015**

angefertigt am

**III. Physikalischen Institut A**

Erstgutachter und Betreuer

Prof. Dr. Thomas Bretz
III. Physikalisches Institut A
RWTH Aachen

Zweitgutachter

Prof. Dr. Thomas Hebbeker
III. Physikalisches Institut A
RWTH Aachen

# Contents

# 1. Abstract

The Pierre Auger Observatory is the world's largest experiment exploring the extensive air showers (EASs) of ultra-high-energy cosmic rays (UHECRs). It is located in the Pampa Amarilla, Argentina, and uses different detectors to study the sources, the mass composition, the energy and the propagation mechanisms of UHECRs.

In order to draw inferences on the mass composition and the energy of UHECRs, it is important to determine the muonic component of an extensive air shower. In the course of the current Pierre Auger Observatory Upgrade, called "AugerPrime", a scintillating surface detector (SSD) is planned to further improve the determination of the muonic component together with the yet existing surface detector (SD).
The SD consists of water Cherenkov tanks (WCTs) and uses photomultiplier tubes (PMTs) to observe Cherenkov light generated by incoming charged particles of the EAS. A prototype of the SSD that is currently used in Argentina is the ASCII detector which consists of several ASCII modules. These modules use PMTs to detect scintillation light generated by secondary particles of the EAS within scintillator bars. The ASCII modules are placed on top of the WCTs to be able to determine the muonic component more precisely than it is possible with the SD alone. This is achieved by superimposing the signal of the ASCII modules and the WCTs, as these two detectors have a different response to the muonic component of an EAS [1].

The III. Phys. Inst. of the RWTH Aachen University proposed to use SiPMs instead of PMTs for the ASCII detector as using SiPMs has several advantages compared to using PMTs. The gain of the SiPMs can be determined from their finger spectrum. This has the advantage that changes of the gain caused by the SiPM can be better distinguished from changes of the gain caused by the scintillator. Moreover SiPMs are optically and mechanically more stable and can be handled easier than PMTs. In so doing, SiPMs provide all the requirements concerning dynamic range, PDE and noise.
As proof of principle, some ASCII modules in Argentina are equipped with SiPMs that are connected to ASCII boards manufactured in Aachen.

A prototype ASCII board is used in this thesis. To be able to determine the SiPM-gains from the traces live, it is essential to have a stable algorithm that creates a finger spectrum. Therefore an algorithm will be developed in this thesis.

# 2. Cosmic Rays and the Pierre Auger Observatory

**Cosmic Rays**

The atmosphere of the Earth is permanently penetrated by high-energy atomic nuclei, the so-called cosmic rays. To detect these particles large experimental challenges arise. The energy spectrum of cosmic rays ranges from few MeV up to $10^{20}$ eV. At the GeV range several thousand particles cross the universe per second and square meter. Due to this high flux these cosmic rays can be examined directly by small detectors in the outer space or close to the atmosphere's border. In order to do this, satellites or balloons equipped with detectors can efficiently be used. As the flux of cosmic rays falls steeply with increasing energies, direct measurements are not feasible anymore for cosmic rays with energies above $10^{14}$ eV. The flux decreases to less than one particle per century and square kilometer for particles with an energy of $10^{20}$ eV. Therefore large detection areas are needed which can only be built on ground level. The motivation to expand such an effort is the interest in the sources, the composition and the propagation mechanisms of high-energy cosmic rays. Especially properties of ultra-high-energy cosmic rays (UHECR) are of great interest. They carry energies above $10^{18}$ eV and their flux is suppressed above $10^{20}$ eV. On the one hand the propagation mechanisms might cause this suppression on the other hand the sources may not be able to inject more energy into the cosmic rays [2].

**Extensive Air Showers**

When these primary particles enter the Earth's atmosphere, they interact with nuclei producing secondary particles, which may interact with nuclei in the atmosphere again or decay. This process is described by an extensive air shower (EAS). During the first interaction mostly pions are created. However, kaons can also be produced. Subsequently photons and muons arise from decays of these mesons [3].
An example of an EAS is shown in figure 2.1, where produced neutrinos are not drawn in. The EAS is divided into the electromagnetic component with photons and electrons, the hadronic component and the muonic component. The yellow shaded area features that these components can merge into each other. Because cosmic rays carry energies much higher than particles in man-made accelerators, the hadronic interactions taking place in an EAS are topic of current research.
The muonic component of an EAS is important for studies of the primary particles. If a detector measures the number and the lateral distribution of the muons in an EAS, it is possible to draw inferences about the composition of the primary particle.

Moreover the muon density on the ground can be used to obtain the energy of the primary particle independent of its mass. Here, a challenge that has to be faced is the distinction of the electromagnetic component from the muonic component as the muonic component cannot be measured directly [2].

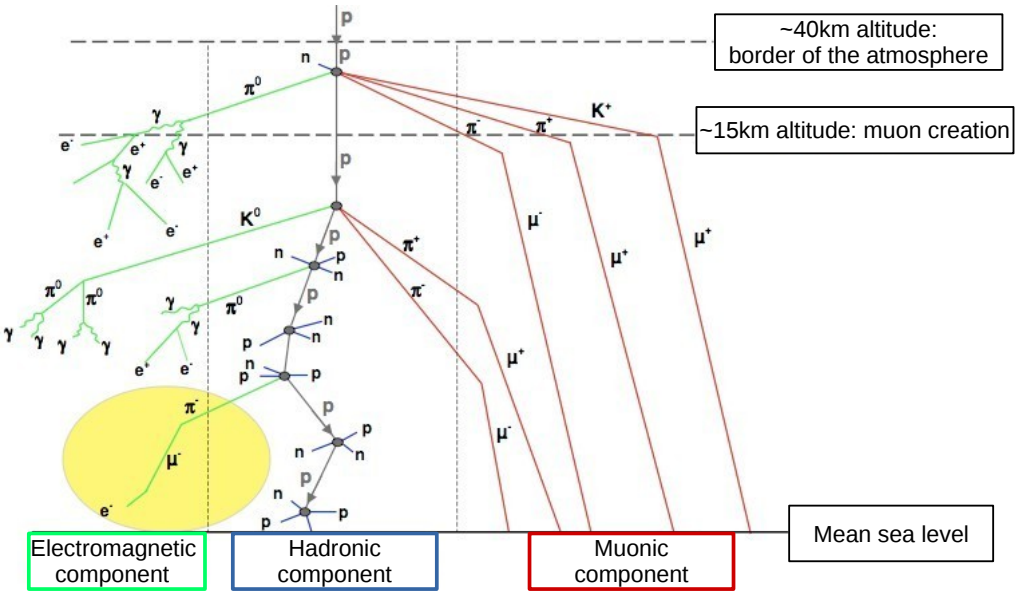


**Figure 2.1:** Components of an extensive air shower. The yellow shaded area features the possibility of transitions between the components. Neutrinos are not drawn in this figure. Adapted from [4].

### The Pierre Auger Observatory

The Pierre Auger Observatory is the largest cosmic ray observatory ever built by human beings. It is located in the Pampa Amarilla near the city of Malargüe in Argentina. The goal of this multinational collaboration is to investigate the sources, characteristics and interactions of cosmic rays with energies above $10^{18}$ eV. Therefore an outstanding hybrid detector is used among other detectors, that cannot all be elucidated in this thesis.

Figure 2.2 shows the design of the observatory. Each dot represents one of the in total 1660 surface detector (SD) stations, which are spread over roughly 3000 $\mathrm{km}^2$ with a spacing of 1.5 km between next neighbours. The SD stations are made of robust polyethylene water Cherenkov tanks (WCT) each housing 12000 l of ultra-pure water and three photomultiplier tubes (PMTs). Therewith they detect Cherenkov light from passing charged particles of the electromagnetic and muonic component of extensive air showers. An advantage of the SD is its duty cycle of almost 100%. Figure 2.2 also shows 24 fluorescence telescopes housed in four enclosures overlooking the SD array. Electromagnetic particles of an extensive air shower excite nitrogen

atoms which in turns emit fluorescence light in the ultraviolet range during their de-excitation. The fluorescence detector (FD) uses the PMT based telescopes to measure this light in dark nights with good weather conditions. So the duty cycle of the FD is limited to roughly 15%. In the hybrid mode data from both, SD and FD, are used simultaneously to obtain information on the footprint and the longitudinal propagation of an extensive air shower [5].

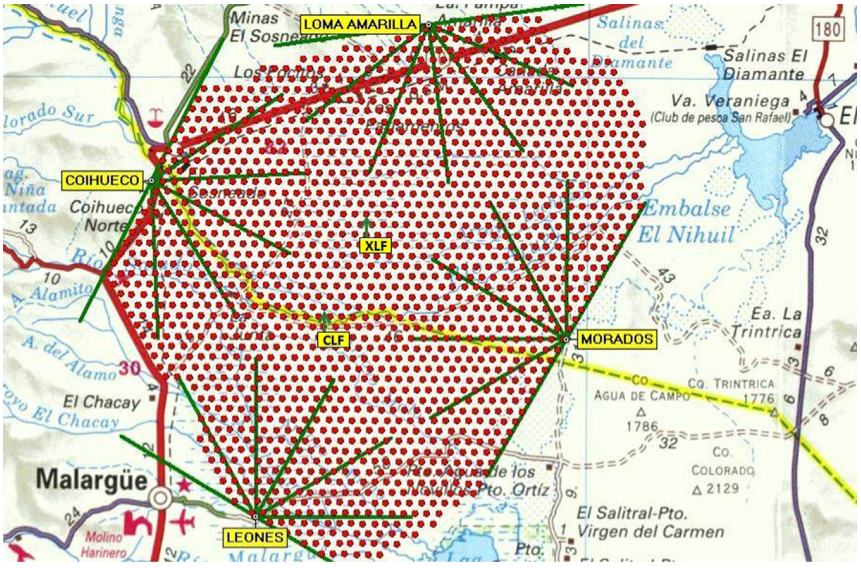


**Figure 2.2:** A map of the Pierre Auger Observatory with its 1660 surface detector stations (dots) and the four fluorescence detector enclosures. The green lines depict the field of view from one fluorescence telescope. Taken from [5].

**AugerPrime - The Upgrade of the Pierre Auger Observatory**

With these methods the Pierre Auger Observatory has already measured EASs very successfully. For a further advancement an upgrade is planned that is called AugerPrime during the start-up phase. The upgrade AugerPrime aims to study the composition and the origin of the flux suppression of highest energetic cosmic rays in more detail. Moreover the contribution of protons to the flux shall be studied up to the highest energies allowing an improved anisotropy study. Furthermore the development of EASs and the hadronic interactions taking place in an EAS have to be elucidated.

To achieve these goals additional Surface Scintillator Detectors (SSD) made of plastic scintillator bars will be placed on top of each SD station. As the SSD is placed above the SD station, the EAS is not shielded as much as for the SD station, such that the ratio of electromagnetic and muonic component differs for these two detectors. Therewith a linear combination of the SSD and the SD station signal enhances the determination of the muonic component whose importance was described in this thesis before. A picture of a SSD prototype installed on a SD station is shown in figure 2.3. To improve the data acquisition and processing of the SD and to allow a communication between the SSD and the SD station, the electronics of the SD stations are upgraded. Moreover the usage of an Underground Muon Detector (UMD)

is planned to obtain direct information on the muonic component. Therewith the UMD shall be a reference and a cross-check possibility for the SSD and the SD. Additionally the duty cycle of the FD will be increased to 20% [1].

One prototype of the SSD is ASCII, the Auger Scintillator for Composition II. ASCII modules are operated since 2010. Like the SSD they consist of two modules covering roughly 2 $m^2$ in total. The light produced by charged particles in the scintillator bars is read out by wavelength-shifting fibers. All the fibers are coupled to a single photo-detector. As stated in [1], PMTs controlled by the Upgraded Unified Board (UUB) are planned to be used for the SSD.
Nevertheless currently three ASCII modules operate with 6x6 $mm^2$ SensL MicroFC-60035-SMT silicon photomultipliers (SiPMs) controlled by the Unified Board (UB), as it was proposed by the III. Phys. Inst. A of the RWTH Aachen University. The front-end board of the SiPM is the ASCII board manufactured at the III. Phys. Inst. A of the RWTH Aachen University. It will be explained in detail in chapter 4.2. The coupling between SiPM and wavelength-shifting fiber consists of a silicone pad and a simple plexiglass cone.
The UB takes data from the SiPM signal of the ASCII board with a sampling rate of 40 MSps. Furthermore the UB filters the incoming signal with a 20 MHz low-pass filter [6]. In this thesis traces of the 6x6$mm^2$ SensL MicroFC-60035-SMT SiPM taken by a prototype of the ASCII board are studied.
Detailed information on the SSD, the UB and the Auger Upgrade in general can be found here [1].

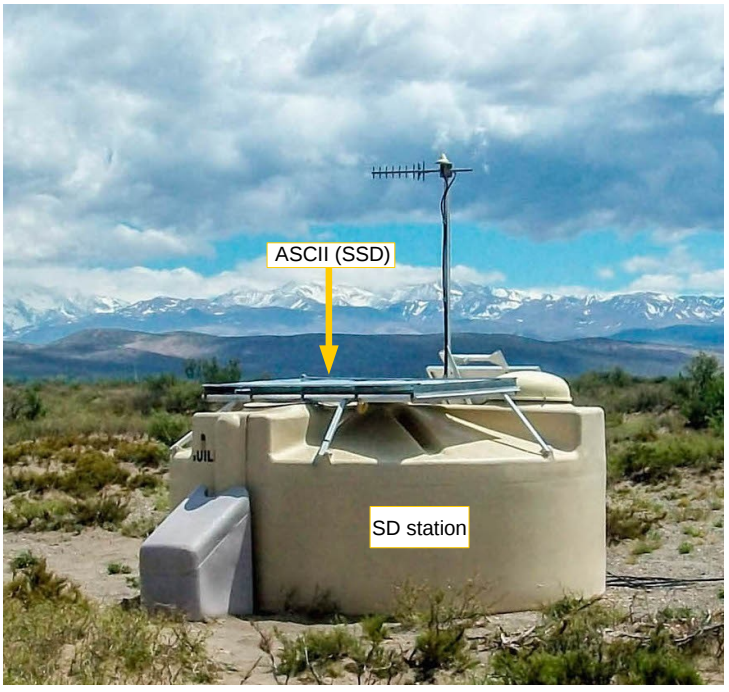


**Figure 2.3:** One of the surface detector stations already equipped with an ASCII module, a SSD prototype. Adapted from [1].

# 3. Silicon Photomultipliers

Due to innovations in recent years, silicon photomultipliers (SiPMs) became a challenging alternative to photomultiplier tubes in astro-particle and particle physics. SiPMs can detect single photons and have a gain and photo detection efficiency (PDE) that are comparable to those of the most efficient PMTs. Moreover SiPMs have several advantages compared to PMTs. They are compact, have a low bias voltage in the range of tens of volts and can be employed undisturbed in magnetic fields. Additionally SiPMs are manufactured cheaply in mass production and operate with simple electronic readout circuits. Moreover SiPMs are mechanically and optically robust.

**From Photodiode to Geiger-mode Avalanche Photodiode**

As silicon is a semiconductor, it has a band gap energy of about $E_G = 1\,\mathrm{eV}$ between the empty conduction band and the valence band. Therefore a photon needs an energy $E_\gamma = h \cdot f \geq E_G$ to excite electrons into the conduction band. To be able to detect photons with lower energies, a photodiode shown in the lower half of figure 3.1 is needed. As shown in the upper half p- or n-doped semiconductors obtain an acceptor level $E_a$ or a donor level $E_d$, respectively. The photodiode consists of a p-n junction whose depletion zone is enlarged by a reverse bias voltage. The gap between valence band and $E_a$ as well as $E_d$ and conductor band is of the order of the thermal energy at room temperature (25 meV). Photons with an energy that is larger than this gap may create electron-hole pairs. Electron and hole are separated by the electric field of the depletion zone and can be detected as a voltage drop. Because of the small energy gap, the photon detection will be superimposed by thermal noise.

This perturbing effect is considerably reduced for avalanche photodiodes. Here the electric field at the junction is stronger so that created electrons gain enough energy to generate electron-hole pairs on their own. Therefore the gain of avalanche photodiodes is 50-200 times larger than the one of photodiodes [7].

In Geiger-mode avalanche photodiodes (G-APDs) the holes have enough energy to create new electron-hole pairs as well. Therefore an avalanche also forms in the p-doped region and therewith in the breakthrough direction. A quenching resistor $R_q$ has to be connected in series with the G-APD to stop this self-sustaining cell breakdown [7].

The gain of a G-APD reaches typically $10^5$ to $10^7$. The amplitude $A_i$ of a G-APD breakdown is proportional to the overvoltage $V_{Ov} = V_{bias} - V_{Bd}$ [7]:

$$A_i \sim \frac{C}{e} \cdot V_{Ov} \ . \tag{3.1}$$

Where $V_{bias}$ is the bias voltage, $V_{Bd}$ the breakdown voltage of the G-APD, $C$ the capacitance of the G-APD and $e$ the elementary charge. After a breakdown the recovery time $\tau \sim R_q \cdot C$ is needed to recharge the G-APD across the quenching resistor. During this time a cell breakdown has a reduced amplitude [7].

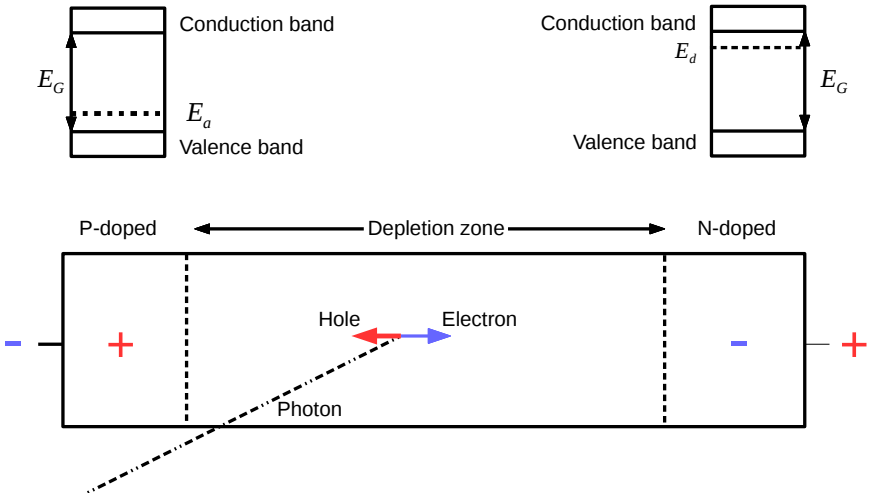


**Figure 3.1:** Schematics of the band structure of doped semiconductors and a p-n junction between p- and n-doped semiconductors with reverse bias voltage.

### Silicon Photomultipliers

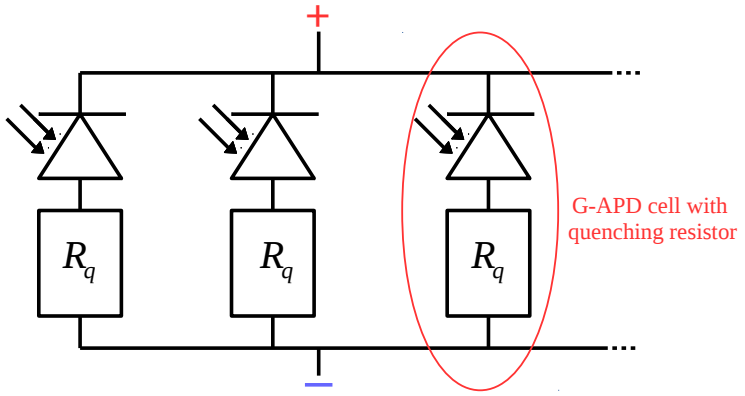


**Figure 3.2:** Self-made equivalent circuit diagram of a SiPM.

An equivalent circuit diagram of a SiPM is shown in figure 3.2. SiPMs consist of many G-APD cells that are connected in parallel electronically. Therefore the amplitude of several cell breakdowns is equal to the sum of the single cell breakdown

amplitudes. The gain of a SiPM is dependent on the overvoltage.
Not only photons can trigger a cell breakdown, but also noise effects. Thermally excited electron-hole pairs that gain enough energy in the internal electric field of the G-APD can trigger cell breakdowns themselves. This process is called thermal noise and increases with the temperature. Furthermore during the avalanche process new photons can be produced. These photons can trigger new breakdowns in the surrounding cells which is called optical crosstalk. The probability for optical crosstalk events rises with the overvoltage. Another noise effect is the afterpulsing. Some electrons or holes are caught in impurities of the silicon. They are released in the range of a few 10 ns later and can cause a new avalanche in the same cell then [7]. Because of innovations over the last few years, the probability for afterpulses decreased heavily as for instance to 0.2% for the two SensL C-Series SiPMs with 35 $\mu$m pitch size used in this thesis [8].
An important performance parameter of photon detectors was mentioned at the beginning of this chapter, the photo detection efficiency (PDE). Neglecting the recovery time of a cell, the PDE can be calculated as the product of the geometric fill factor, the probability that a photon causes a breakdown and the quantum efficiency [7]. The quantum efficiency depends on the wavelength of the photon and peaks in the violet-blue-range for most SiPMs and especially for the SiPMs used in this thesis. Because of the Geiger-mode, the probability that a photon triggers an avalanche amounts to almost 100% for typically used overvoltages. The geometric fill factor is limited by the place needed for the quenching resistors and the desired value of the crosstalk probability. The more space is filled between two neighbouring cells, the more potential crosstalk photons can be absorbed outside of the active area of the SiPM.

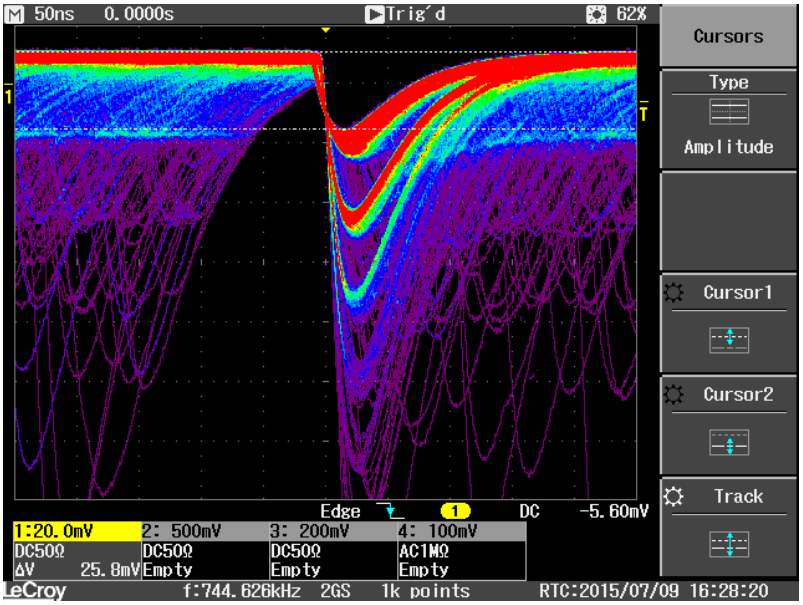


**Figure 3.3:** Noise signal of SensL MicroFC-SMTPA-30035 SiPM processed and amplified by laboratory board. Screenshot taken by LeCroy WaveJet 354A oscilloscope with 50 Ω load and color-coded event rate. Voltage (div=20 mV) is plotted against time (div=50 ns).

The SiPMs used in this thesis are the SensL MicroFC-SMTPA-30035 and MicroFC-60035-SMT as well as the Hamamatsu MPPC S12571-100C. Their important specifications provided by the manufacturers are given in table 3.1. The specifications are given at a temperature of 21 °C and an overvoltage of 2.5 V for the SensL models and 25°C and 1.4 V for the Hamamatsu models, respectively. Furthermore all the given PDEs do not contain the noise effects of optical crosstalk or afterpulsing. Additionally the PDEs are given at the peak wavelength which amounts to $\lambda_p = 420\,\text{nm}$ for the SensL manufactured SiPMS [8] and $\lambda_p = 450\,\text{nm}$ for the one of Hamamatsu [9], respectively.
In figure 3.3 a noise signal of the SensL MicroFC-SMTPA-30035 SiPM processed and amplified by the laboratory board is shown. The smallest pulse corresponds to a single cell breakdown. As one can clearly see, the amplitude of the SiPM signals are a multiple of the single cell breakdown though there are small fluctuations in the pulse amplitude. A possible explanation for these fluctuations is the fluctuation of the gain that is for instance caused by the individual capacitance of a SiPM cell.
As the detection of a photon generates a single cell breakdown, henceforth, cell breakdowns will be called photon equivalents (p.e.).

| Manufacturer | SensL | | Hamamatsu |
|---|---|---|---|
| Temp. and $V_{Ov}$ | 21 °C, 2.5 V | | 25 °C, 1.4 V |
| Model | MicroFC-SMTPA-30035 | MircoFC-60035-SMT | MPPC S12571-100C |
| Sensor size | 3x3 $\text{mm}^2$ | 6x6 $\text{mm}^2$ | 1x1 $\text{mm}^2$ |
| Cell / Pitch size | 35 $\mu$m (cell) | 35 $\mu$m (cell) | 100 $\mu$m (pitch) |
| Number of cells | 4774 | 18980 | 100 |
| Fill factor | 64% | 64% | 78% |
| PDE at $\lambda_p$ | 31% | 31% | 35% |
| Gain | $3{\cdot}10^6$ | $3{\cdot}10^6$ | $2.8{\cdot}10^6$ |
| 0.5 p.e. dark noise | 300 kHz | 1200 kHz | 100 kcps |
| $\beta$ | 21.5 $\text{mV}(^\circ\text{C})^{-1}$ | 21.5 $\text{mV}(^\circ\text{C})^{-1}$ | 60 $\text{mV}(^\circ\text{C})^{-1}$ |
| Optical crosstalk | 7% | 7% | 35% (*) |

**Table 3.1:** Specifications of the SiPMs given by the manufacturers SensL [8] and Hamamatsu [9], respectively. (*) denotes that the value had to be estimated from a plot of optical crosstalk against overvoltage. $\beta$ represents the temperature dependence of the breakdwon voltage ($V_{Bd}(T) = V_{Bd}(T_0) + \beta \cdot (T - T_0)$).

# 4. Experimental setup

As the purpose of this thesis is to extract SiPM pulses from recorded traces, the SiPM has to be placed in darkness. Otherwise photons would continuously reach the SiPM and cause continuous cell breakdowns in its G-APDs. Therewith signal extraction on a single p.e. basis would not be possible. According to that, a dark box is used.
The experimental setup is shown in figure 4.1.

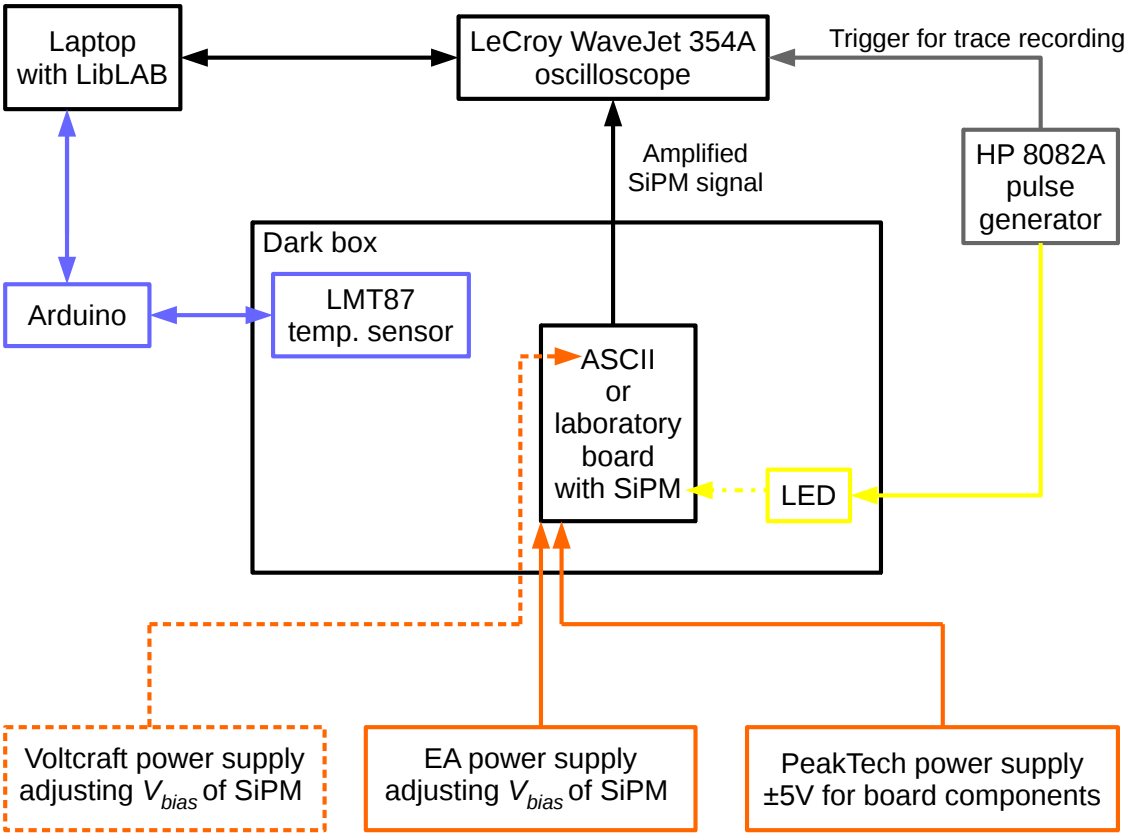


**Figure 4.1:** Schematic of the experimental setup. The power supply in the dashed box is only operated with the ASCII board. The temperature measurement module (blue boxes; Arduino and temp. sensor) is only used for the Hamamatsu and the SensL 6x6 mm$^2$ SiPM. Moreover, the LED is solely used for the determination of the breakdown voltage of these two SiPMs, see next two chapters. "LibLAB" is a laboratory software framework, developed locally at III. Phys. Inst. A and B [10].

## 4.1 Test measurements with laboratory board

Before the main measurement with the ASCII board took place, test measurements were performed. Therefore once the SensL 3x3 $mm^2$ MicroFC-SMTPA-30035 SiPM and another time the Hamamatsu 1x1 $mm^2$ MPPC S12571-100C SiPM is connected to the laboratory board. A description of these SiPMs was given at the end of chapter 3. As SiPM traces taken in darkness are to be analysed, laboratory board and connected SiPM are placed in a dark box.

**The laboratory board**
The laboratory board has been developed by J. Schumacher in his master's thesis [11]. The bias voltage of the SiPM is applied by an external power supply and filtered by two RC low pass filters. To buffer high frequencies and therewith short and high noise pulses generated by the SiPM, the second RC element includes an additional small capacitance.
A transimpedance amplifier is used for an active current-to-voltage conversion of the SiPM signal. The transimpedance amplifier consists of a feedback resistance of $R_f = 4.7\,\mathrm{k\Omega}$ and an intersil EL5165 operational amplifier (op-amp) with a $-3\,\mathrm{dB}$ bandwidth of 600 MHz and a slew rate of $4700\,\mathrm{V}\mu\mathrm{s}^{-1}$ [12]. The frequency response of the op-amp, i.e. its bandwidth and slew rate, degrades with increasing feedback resistance. Nevertheless such a high value of $R_f$ is used because it is directly proportional to the gain of the amplification. Moreover with the limited bandwidth of the op-amp at a high gain the high frequencies of the white noise are cut which increases the signal to noise ratio. Hence a high gain amplification from the single p.e. signals, i.e. the SiPM current $I_{SiPM}$, to the output voltage $V_{out}$ is achieved:

$$V_{out} = -R_f \cdot I_{SiPM} \ . \tag{4.1}$$

This amplified output signal can be accessed via a LEMO connector.

**EA-PSI 6150-01 DC power supply**
This power supply manufactured by Elektro-Automatik applies the bias voltage for the SiPM. The voltage $V_{set} \equiv V_{bias}$ can be set in a range of 0 V to 150 V with a resolution of 10 mV. At temperatures of $(25 \pm 5)\,^{\circ}\mathrm{C}$ the voltage accuracy is stated to be smaller than:

$$\Delta V_{set} < 0.05\% \cdot V_{set} + 10\,\mathrm{mV} \quad [13]. \tag{4.2}$$

As this accuracy is not denoted to be a standard deviation, it will not be taken into account for the analysis. Therefore the standard deviation of $V_{bias}$ will be estimated for the SensL SiPM. For the Hamamatsu SiPM and the measurements with the ASCII board (see next chapter 4.2) an Agilent multimeter is used to measure $V_{bias}$ and to estimate its standard deviation.

**PeakTech 6035D DC power supply**
This regulated laboratory power supply has a 12 V and a 5 V output as well as an

output that is adjustable in the range of 0 V to 30 V [14]. The adjustable and the 5 V output are used to apply ±5 V to the op-amp of the laboratory board. Therefore the accuracy of this power supply is not necessarily needed to be stated.

**LeCroy WaveJet 354A oscilloscope**
The 500 MHz digital oscilloscope WaveJet 354A manufactured by LeCroy reads the amplified SiPM signal from the laboratory board via one of its four channels. Each channel has a vertical resolution of 8-bit and a DC gain accuracy of $\pm(1.5\% \cdot V_{out} + 0.5\% \cdot \text{full range})$. $V_{out}$ denotes the output voltage of the laboratory board (see equation (4.1)) or of the ASCII board, respectively. The DC gain accuracy influences the vertical scale parameter of the oscilloscope and has its worst-case impact on the data point at the full range. The full range consists of eight vertical divisions. For the recording of traces a vertical sensitivity of $20\,\text{mV(div)}^{-1}$ was chosen for the SensL 3x3 mm$^2$ SiPM and $10\,\text{mV(div)}^{-1}$ for the Hamamatsu 1x1 mm$^2$ SiPM, respectively. For the measurement with the ASCII board and the SensL 6x6 mm$^2$ SiPM a vertical sensitivity of $50\,\text{mv(div)}^{-1}$ was chosen. Therewith the worst-case deviation caused by the DC gain accuracy $\Delta V_{scale}^{max}$ and the digitisation $V_{digi}$ are to be calculated via:

$$\Delta V_{scale}^{max} = \frac{2\% \cdot \text{full range}}{2^8} \,, \tag{4.3}$$

$$V_{digi} = \frac{\text{full range}}{2^8} \,. \tag{4.4}$$

These two equations lead to the values for all the three used SiPMs in table 4.1.

| Board | Laboratory board | | ASCII board |
|---|---|---|---|
| SiPM | Hamamatsu 1x1 mm$^2$ | SensL 3x3 mm$^2$ | SensL 6x6 mm$^2$ |
| $V_{vertical}$ | $10\,\text{mV(div)}^{-1}$ | $20\,\text{mV(div)}^{-1}$ | $50\,\text{mV(div)}^{-1}$ |
| $\Delta V_{scale}^{max}$ | 0.00625 mV | 0.0125 mV | 0.03125 mV |
| $V_{digi}$ | 0.3125 mV | 0.625 mV | 1.5625 mV |

**Table 4.1:** Worst-case DC gain accuracy $\Delta V_{scale}^{max}$ (equation (4.3)) and digitisation $V_{digi}$ (equation (4.4)) of the oscilloscope for the vertical sensitivity $V_{vertical}$ of each analysed SiPM.

As even in the worst case the DC gain accuracy is smaller than the digitisation, it is neglected. The digitisation is taken into account to choose the binning in the finger spectra of the analysis chapters.
The time base accuracy of the oscilloscope amounts to 10 ppm and refers to the inverse sampling rate. For both SiPMs a time division of 100 $\mu$s was chosen which corresponds to a sampling rate of $500\,\text{MSs}^{-1}$. Therefore, each sample has a time accuracy of 0.02 ps.
The oscilloscope is controlled and read-out by a laptop via an Ethernet connection. Moreover, an external trigger from a pulse generator is applied to a channel for the

recording of SiPM traces [15].

**HP 8082A pulse generator**
One of the two outputs of the HP 8082A pulse generator is connected to a channel of the oscilloscope to trigger the recording of a SiPM trace in single-shot mode. Therefore the traces are triggered randomly. For the preliminary determination of the breakdown voltage of the Hamamatsu SiPM (see chapter 4.3), the pulse generator also serves to pulse the Lumitronix LED. The pulsed LED increases the SiPM signal but does not evoke a saturation of the high gain transimpedance amplifier. Thus the breakdown voltage is determined more precisely with the pulsed LED than in darkness.
Pulse width, repetition rate and amplitude of the pulse generator are adjustable. Further specifications are not required for the above mentioned applications but can be found in [16].

**Lumitronix superbright LED UV**
This Lumitronix LED is used as it has a peak wavelength of 407 nm which is close to the peak wavelength of all used SiPMs [17].

**Laptop with LibLAB**
The Laptop is connected to the oscilloscope via Ethernet and is used to adjust and readout the oscilloscope with self-written C++ programs based on the "LibLAB" [10]. The laboratory software framework "LibLAB", developed locally at the III. Phys. Inst. A and B, provides an easy access to the oscilloscope as well as to several laboratory hardware [10].
For the Hamamatsu SiPM the laptop also controls the Arduino which is used to control the temperature sensor LMT87.

**Arduino Uno micro-controller board**
Therefore a self-written C++ program using the open source Arduino software is used. The laptop and the Arduino Uno board are connected via USB. This micro-controller board houses a 5 V output pin as well as six analogue input pins which measure voltages in the range of 0 V to the voltage of an analogue reference pin $A_{ref}$. As described in chapter 4.3, this reference voltage is measured and calibrated with the Agilent multimeter to achieve a more precise value than the stated value of 5 V. The analogue-to-digital converter (ADC) of the integrated Atmel micro-controller ATMEGA 328P-PU is used to digitise the voltages at the analogue input pins [18]. The resolution of the ADC amounts to 10-bit, where the minimum value represents ground and the maximum value represents the voltage of $A_{ref}$ minus one LSB [19]. The temperature sensor LMT87 is supplied with the 5 V output pin of the Arduino Uno board and read out by an analogue input pin. For the readout the "analogRead()" function of the Ardunio software is used. This function uses the ADC to convert the input voltage into channel numbers *ch* between 0 and 1023. As for this process roughly 100 $\mu$s are needed, same temperature values were not measured

more than once by the self-written program that reads the voltage of the temperature sensor with a minimal time gap of 100 ms [20]. The digitised voltage $V_{ard}$ is to be calculated via the voltage of the analogue reference pin $V_{ref}$ and the channel number of the ADC $ch$:

$$V_{ard} = \frac{V_{ref} \cdot ch}{1024} \ . \tag{4.5}$$

**Texas Instruments LMT87 temperature sensor**
The LMT87 manufactured by Texas Instruments is an analogue temperature sensor for a temperature range of -50 °C to 150 °C. For supply voltages between 3.4 V and 5.5 V and within an ambient temperature spanning from 20 °C to 40 °C, an (worst-case) accuracy of ±0.3 °C is achieved [21]. The temperature $T$ for a given sensor voltage $V_T$ is to be calculated with the transfer function:

$$T\,[^\circ\mathrm{C}] = \frac{13.582 - \sqrt{(13.582^2 + 4 \cdot 0.00433 \cdot (2230.8 - V_T[\mathrm{mV}])}}{-2 \cdot 0.00433} + 30 \quad [21]. \tag{4.6}$$

The stated accuracy and transfer function are used in chapter 5.1, where the temperature measurement is analysed.

**Agilent U1232A digital multimeter**
As described above, this multimeter is used to measure DC voltages in the experiments with the Hamamatsu 1x1 mm$^2$ SiPM connected to the laboratory board and the SensL 6x6 mm$^2$ SiPM connected to the ASCII board. Thereby the digitisation of the multimeter amounts to 1 mV and 10 mV for measured voltages in the range of 6 V and 60 V, respectively [22].
The DC voltage accuracy of the multimeter is estimated for each measurement.

## 4.2 Measurements with the ASCII board

The main measurement is carried out with the SensL 6x6 mm$^2$ MircoFC-60035-SMT SiPM connected to the prototype of an ASCII board. Therewith the same constellation as in three SSD prototype ASCII modules at the Pierre Auger Observatory in Argentina is used. The experimental setup is almost equal to the one of the measurements with the Hamamatsu SiPM connected to the laboratory board. Only the voltage supply for the ASCII board differs from the setup (see figure 4.1).

**The ASCII board**
The prototype ASCII board, used in this thesis, was developed at the III. Phys. Inst. A of the RWTH Aachen University. In the following the components of the ASCII board will be described. Thereto a picture of the ASCII board is shown in figure 4.2.
In Argentina the UB applies 12 V to the ASCII board via the UB connector. As the components of the ASCII board are operated at different voltages, three regulators in the white dashed box close to the UB connector are used. A linear regulator uses the 12 V to generate +5 V for a linear regulator (circle in the middle of the picture),

that was developed at the III. Phys. Inst. A of the RWTH Aachen University to produce the bias voltage for the SiPM. Another linear regulator generates +3.3 V for the digital components of the board. A switching regulator, generating ±5 V for the preamplifier on the left of the board, was removed in Argentina because it caused switching noise. Instead, low noise ±3.3 V from the UB was used.
Another switching regulator placed on a board is connected to the ASCII board in the middle of the picture. It is used to generate 40 V for the input voltage of the linear regulator that regulates the bias voltage of the SiPM controlled by a micro-controller. As a temperature sensor is placed close to the SiPM and readout by the micro-controller, the linear regulator is able to correct the temperature dependence of the breakdown voltage.
The 6x6 $mm^2$ SensL MicroFC-60035-SMT SiPM is placed on a base board that is connected to the ASCII board, shown in figure 4.3. The signal of the SiPM passes the preamplifier and can be readout via a high and a low gain LEMO output.

As the high gain output is designed for a single p.e. resolution, it is used in this thesis and connected to the oscilloscope. The three regulators in the white dashed box are not installed on the ASCII board used here just as the board with the switching regulator. Moreover the digital components like the temperature sensor and the micro-controller are not operated.
Therefore three power supplies have to be used instead of only one as in Argentina and the temperature correction cannot be performed. As with the measurements with the laboratory board, the PeakTech 6035D DC power supply is used to apply ±5 V to the preamplifier of the ASCII board. The EA-PSI 6150-01 DC power supply applies 35 V to the linear regulator that generates the bias voltage of the SiPM. The regulation is achieved via the Voltcraft DPS-8003PFC power supply.

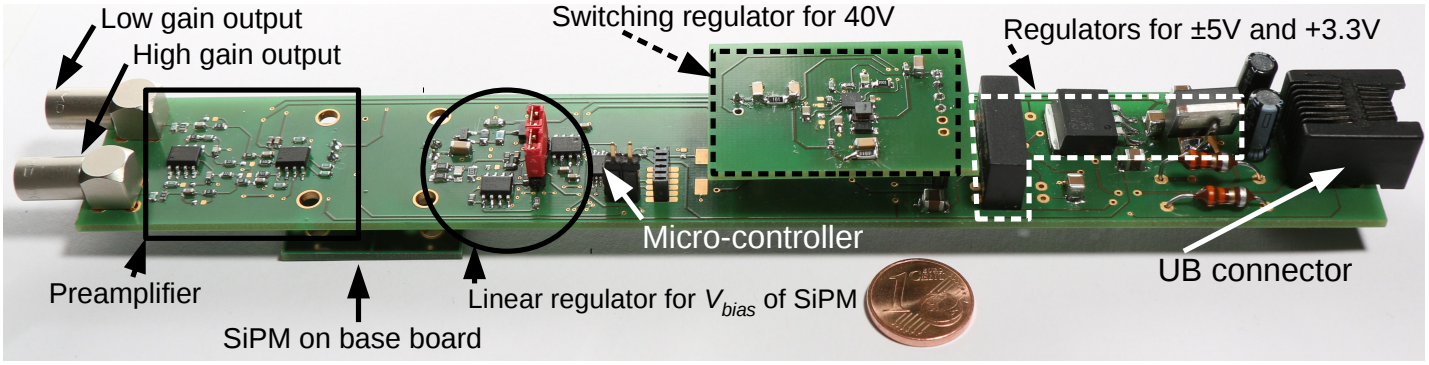


**Figure 4.2:** Picture of the ASCII board used in this thesis. The board has a length of about 200 mm. The regulators in the dashed boxes were replaced by using three power supplies with different operating voltages (see figure 4.1) instead of a single 12V source like the one of the UB in Argentina. Photo courtesy of L. Middendorf (III. Phys. Inst. A, RWTH Aachen).

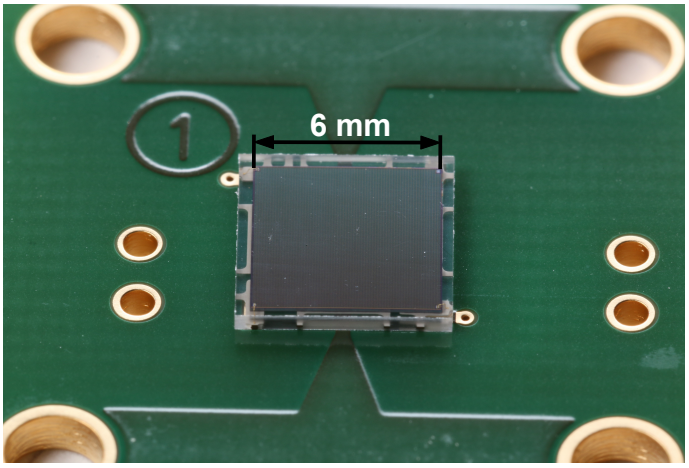


**Figure 4.3:** Picture of the SensL 6x6 mm$^2$ MicroFC-60035-SMT SiPM placed on a base board that is connected to the ASCII board as shown in figure 4.2. Photo courtesy of L. Middendorf (III. Phys. Inst. A, RWTH Aachen).

**Voltcraft DPS-8003PFC power supply**
The Voltcraft DPS-8003PFC is a switching power supply. However, 50 Hz noise is visible at the output coming from the 230 V AC / 50 Hz mains. Therefore a self-constructed pi-shaped RC low pass is placed between it and the ASCII board. An RC low pass was chosen because this power supply only generates a reference voltage for a linear regulator such that there does not flow any current. The low pass comprises a reservoir capacitance of 1000 $\mu$F, a resistance of $R = 267\,\Omega$ and a smoothing capacitance of $C = 560\,\mu$F. Consequently the cutoff frequency of the low-pass amounts to $f_C = \frac{1}{2\pi \cdot R \cdot C} \approx 1\,Hz$ and the 50 Hz noise is filtered out. An error estimation is renounced for this estimate.
The output voltage of this Voltcraft power supply can be set from 0 V to 80 V and in 10 mV steps [23]. Because this voltage is scaled up by the linear regulator of the ASCII board before it reaches the SiPM, the bias voltage of the SiPM can only be arranged with a step size of about 0.2 V. The error on the bias voltage of the SiPM is estimated from measurements with the Agilent multimeter as described in the next chapter.

## 4.3 Measurement procedure

For each SiPM the **breakdown voltage** was preliminary determined at the beginning of the measurement procedure. This was performed by setting a bias voltage at which the SiPM signal is clearly visible like in figure 3.3. Therewith a bias voltage of roughly 30 V was applied to the SensL SiPMs and roughly 66 V to the Hamamatsu SiPM, respectively. Then the bias voltage was slowly decreased such that the gain of the SiPM pulses got smaller until the pulses could not be differentiated from the noise of the baseline. At this point the applied bias voltage is expected to equal the breakdown voltage.
For the measurement with the Hamamatsu 1x1 mm$^2$ SiPM, connected to the laboratory board, and the main measurement with the SensL 6x6 mm$^2$ SiPM, connected

to the ASCII board, the pulsed LED was used additionally. Therewith the breakdown voltage is determined more exactly because of the reasons described in chapter 4.1. A pulse repetition rate of about 500 Hz was chosen and the pulse amplitude was adjusted individually for each SiPM to values of roughly 3 V, such that continuous cell breakdowns as well as a saturation of the amplifiers on the boards were avoided. When the breakdown voltage was found, the SiPMs were disconnected to measure the voltage directly at the contact points on the board. Therefore the Agilent multimeter was used. During the measurements with the SensL 3x3 $mm^2$ SiPM with the laboratory board were carried out, some devices were not available, such that the LED was not used and the breakdown voltage was read out from the display of the EA-PSI 6150-01 DC power supply. The error on the breakdown voltage was estimated individually for each SiPM.

Thereafter **SiPM traces** were recorded in darkness and at different overvoltages for all the SiPMs. The bias voltages and their errors were determined analogous to the measurement of the breakdown voltage.
Negative pulses with a width of a few nanoseconds, a repetition rate of about 500 Hz and an amplitude of about 400 mV were generated by the HP pulse generator. With the "LibLAB" based program on the laptop, the trigger of the oscilloscope was set to -350 mV in the falling edge and single-shot mode.
Several test measurements with differently adjusted time and voltage sensitivities of the oscilloscope were performed and analysed to find the best settings. The time sensitivity was chosen such that the recorded trace contains as many SiPM pulses as possible. Here the maximal length of the traces was limited by the finite sampling rate of the oscilloscope. The voltage sensitivity and voltage offset were chosen such that the digitisation has a small influence on the single p.e. pulses while as many p.e. heights as possible fit into the full range. The results for the vertical, i.e. voltage, sensitivity were stated in table 4.1, the time division for both SiPMs used with the laboratory board was chosen to be 100 $\mu$s and 200 $\mu$s for the main measurement with the ASCII board. As the horizontal, i.e. time, axis of the oscilloscope houses 10 divisions, this leads to trace lengths of 1 ms and 2 ms, respectively. As the oscilloscope is only able to save 500 k samples, the sampling rate amounts to 500 MSps and 250 MSps, respectively.
With these settings 30 traces per overvoltage were recorded for the SensL SiPMs. 60 traces were recorded for each overvoltage of the Hamamatsu SiPM because of the low dark noise rate.

During the recording of the SiPM traces for each overvoltage and the preliminary determination of the breakdown voltage, **temperature measurements** were performed for the Hamamatsu SiPM and the SensL 6x6 $mm^2$ SiPM of the main measurement. Thereto the Arduino was used to readout the voltage of the analogue temperature sensor and send the corresponding digitised channel value to the laptop, where it is saved. The temperature sensor was placed in the dark box and close to the laboratory or ASCII board.
Before the measurements with the two SiPMs were carried out, a calibration meas-

urement was performed to calibrate the reference voltage of the Arduino. For a few minutes a channel value was recorded every 100 ms such that roughly 3000 channel values were saved. During this procedure the output voltage of the temperature sensor was measured with the Agilent multimeter. The measured voltage was constant with $V_{Mm}$ =2.341 V such that the temperature was estimated to be constant during the whole calibration measurement.
As the measurement of the breakdown voltage with the Agilent multimeter only needs a few seconds, the temperature was measured 100 times with a spacing of 100 ms. Therewith the temperature is measured over 10 s. As described in the following chapter this group of 100 channel values is averaged to obtain the temperature from the breakdown voltage measurement.
The oscilloscope takes a few minutes to record 30 or even 60 SiPM traces. Therefore the explained temperature measurement is repeated every minute and again the groups of 100 channel values are averaged. Therewith the temperature is determined every 65 s (see next chapter).
The ambient temperature during the SensL measurements could only be determined with a coloured alcohol thermometer.

# 5. Analysis

## 5.1 Temperature measurement

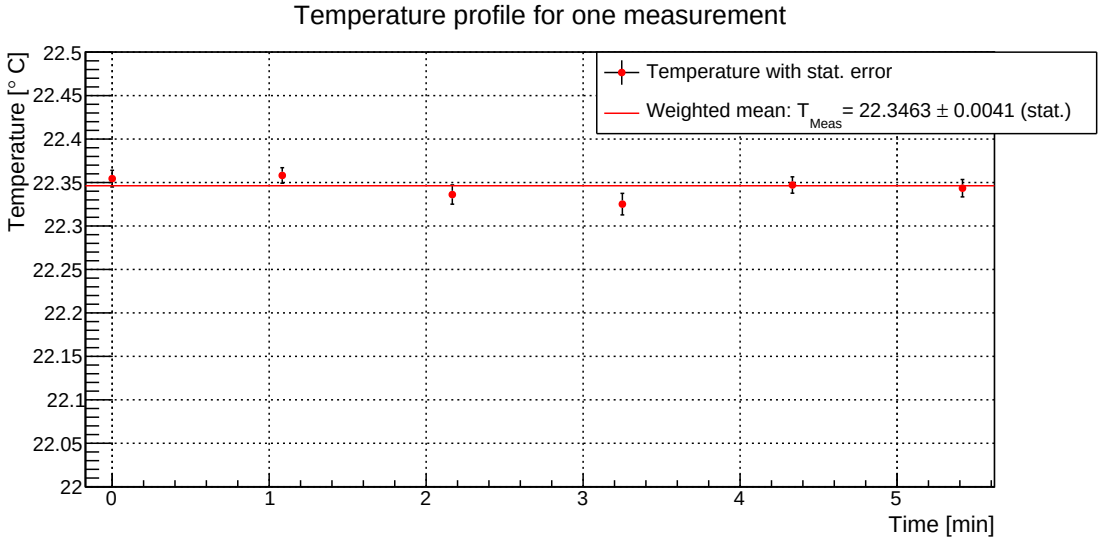


**Figure 5.1:** Example of a temperature profile. Measured during the 30 trace recordings for $V_{bias} = 28.87\,\mathrm{V}$ of the SensL 6x6 mm$^2$ SiPM connected to the ASCII board. Each red dot represents the arithmetic mean of 100 temperature measurements taken within 10 s. The error bars represent the standard deviation of the arithmetic mean.

At first it is to say that all the measurements were carried out in the same room. The room is air-conditioned to a temperature of about 22 °C such that the temperature is not expected to vary more than about 1 K. Especially during the calibration measurement and within the 10 s of the 100 temperature measurements, the temperature is assumed to be constant. This was verified by random test measurements of the temperature sensor voltage with the Agilent multimeter.
Hence the mean of the channel values of the calibration measurement $\langle ch \rangle$ is calculated to calibrate the reference voltage of the Arduino $V_{ref}$. The error on the derived value is calculated via the error on the mean $\sigma_{\langle ch \rangle}$. The error on the temperature sensor voltage measured with the multimeter $V_{Mm} \pm \sigma_{V_{Mm}} = (2.341 \pm 0.002)\,\mathrm{V}$ is

estimated. Moreover $V_{Ard}$ is replaced with $V_{Mm}$ in equation (4.5). Therewith and with a propagation of error on equation (4.5) one obtains:

$$V_{ref} = \frac{V_{Mm} \cdot 1024}{\langle ch \rangle} \pm V_{ref} \sqrt{\left(\frac{\sigma_{\langle ch \rangle}}{\langle ch \rangle}\right)^2 + \left(\frac{\sigma_{V_{Mm}}}{V_{Mm}}\right)^2} \ . \tag{5.1}$$

The statistical error on $V_{ref}$ causes a systematic error on the temperature that is calculated with the transfer function $T(V_T)$ of the temperature sensor LMT 87 (see equation (4.6)). This systematic error will not be factored in until the final temperatures for each SiPM are calculated.
Now the transfer function $T(V_T)$ is used to calculate the temperatures from each saved Arduino channel value $ch_i$. Thereto, $V_T$ is replaced as follows:

$$V_T = \frac{V_{ref} \cdot ch_i}{1024} \ . \tag{5.2}$$

As the temperature is assumed to be constant for each group of 100 measurements, the mean and the error on the mean, i.e. the statistical error, are calculated. These temperature values are plotted against the time for each overvoltage to ascertain that the temperature was constant within the statistical errors during the recording of the SiPM traces. An example for the SensL 6x6 mm$^2$ SiPM connected to the ASCII board is shown in figure 5.1. As one can see, the fluctuation is smaller than 0.05 °C and may be explained with the statistical errors. This is the case for all the trace recordings. Therefore the weighted mean and the error on the weighted mean are calculated which is drawn in the figure, too. The obtained temperature value $T_{Meas}$ is assumed to be the temperature of the SiPM within the complete trace recording process.
Subsequently the obtained temperature values of the breakdown voltage measurement and the trace recordings of all the overvoltages are compared for each SiPM. The maximal temperature deviation amounts to 0.07 °C for the SensL 6x6 mm$^2$ and 0.01 °C for the Hamamatsu 1x1 mm$^2$ SiPM, respectively. To estimate the influence of this temperature deviation on the gain of the SiPMs, the temperature dependence of the breakdown voltage $V_B(T)$ (see table 3) and the direct proportionality between the overvoltage and the gain of an SiPM are used. The gain changes by 1% as the temperature changes by $\frac{1\% \cdot V_{Ov}}{\beta}$. Therewith the temperature affects the gain the most if the overvoltage is the smallest. The smallest overvoltage of the SensL 6x6 mm$^2$ amounts to 3.85 V (see chapter 5.6) and 0.6 V for the Hamamatsu 1x1 mm$^2$ SiPM (see chapter 5.5), respectively. As a consequence, the deviation of the temperature has to be smaller than about 1.8 °C for the SensL 6x6 mm$^2$ SiPM and 0.1 °C for Hamamatsu 1x1 mm$^2$ SiPM to achieve a gain stability of 1%.
Hence the measured maximal temperature deviations of 0.07 °C for the SensL 6x6 mm$^2$ and 0.01 °C for the Hamamatsu 1x1 mm$^2$ SiPM have negligible influence on the gain. Because of that the mean of all $T_{Meas}$ values $T_{SiPM}$ is determined for each SiPM and assumed to be the temperature of the whole measurement.
The statistical error on $T_{SiPM}$ is determined via a propagation of error with the digitisation of the Arduino channels $\sigma_{ch}^{digi} = \frac{1}{\sqrt{12}}$ because the errors on each $T_{Meas}$ and the error on the mean $T_{SiPM}$ are negligible. The systematic errors are on the

one hand the 0.3 °C stated in the datasheet of the LMT87 temperature sensor [21] and on the other hand the error on $V_{ref}$ that is also included via a propagation of error. The 0.3 °C error of the LMT87 sensor is not given as a standard deviation and therefore not included in the final equations below.
As during the measurements with the SensL 3x3 mm$^2$ SiPM some devices were not available, the temperature was only readout from a coloured alcohol thermometer that was placed nearby the SiPM. During the whole measurement with this SiPM, the readout temperature was $T_{SiPM} = 22\,°\text{C}$. The statistical error on the temperature is estimated with the scale error of $\frac{1}{\sqrt{12}}\,°\text{C}$ and rounded to one significant digit. The error on the absolute temperature is estimated to be $0.5\,°C$ and used as systematic error. This yields the following final results of the temperature measurement.

SensL 3x3 mm$^2$ with laboratory board:

$$T_{SiPM} = (22.0 \pm\ 0.3\ (\text{stat.})\ \pm\ 0.5\ (\text{syst.}))\,°\text{C}\ . \tag{5.3}$$

Hamamatsu 1x1 mm$^2$ with laboratory board:

$$T_{SiPM} = (22.37\ \pm\ 0.11\ (\text{stat.})\ \pm\ 0.15\ (\text{syst. V}_{\text{ref}}))\,°\text{C}\ . \tag{5.4}$$

SensL 6x6 mm$^2$ with ASCII board:

$$T_{SiPM} = (22.32\ \pm\ 0.11\ (\text{stat.})\ \pm\ 0.15\ (\text{syst. V}_{\text{ref}}))\,°\text{C}\ . \tag{5.5}$$

## 5.2 Signal extraction algorithm

In this thesis SiPM pulses are to be extracted from SiPM traces to obtain so-called finger spectra by saving the pulse heights into histograms. On that account, a signal extraction algorithm is needed. This algorithm will be described in the following. The algorithm program as well as all the other programs used in the analysis of this thesis are written in Python and use PyROOT to create plots and fits.

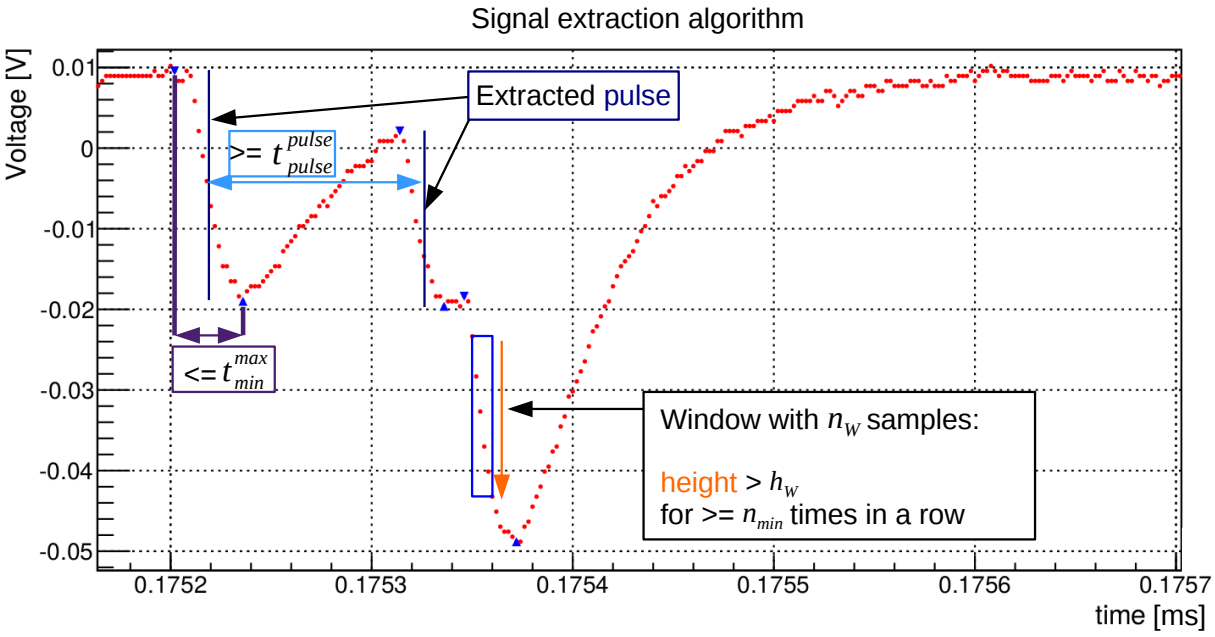


**Figure 5.2:** Zoom into a recorded SensL 3x3 mm$^2$ SiPM trace taken by laboratory board. The small blue triangles mark extracted pulse minima and maxima. Included is a schematic description of the used signal extraction algorithm that is based on windows moving through the trace. Only the cuts that are used for all the SiPMs are drawn in. The left pulse is a single p.e. A more detailed description of the algorithm is given in this chapter.

**The basis of the algorithm**

The implemented algorithm is based on the algorithm developed by M. Lauscher in his master's thesis [24]. The algorithm of M. Lauscher was also used in a modified way by M. Stephan in his doctoral thesis [25]. A picture of an extract of a recorded SensL 3x3 mm$^2$ SiPM trace taken by laboratory board is shown in figure 5.2.
The purpose of the algorithm is to extract the height of SiPM pulses. Therefore the maximum and minimum of the SiPM pulses have to be found. As the SiPM pulses are negative pulses, the maximum denotes the sample at which the steeply falling edge of the pulse begins, i.e. the baseline. The minimum denotes the peak of the negative SiPM pulse. For instance "smaller" is implied to be mathematically smaller whereas heights are always defined to be positive. The algorithm uses windows comprising $\boldsymbol{n_W}$ samples. The position of the window is increased by one sample until the end of the trace is reached. The window is chosen instead of comparing consecutive samples because the latter is more sensitive to noise.

If the last sample of the window is located more than $\boldsymbol{h_W}$ volts under the first sample, it is assumed that the window is located in the falling edge of a SiPM pulse. The value of a counter is raised to measure how many times in a row the height $h_W$ is exceeded and the window position is increased. This is done until $h_W$ is not exceeded anymore. If $h_W$ was exceeded for at least $\boldsymbol{n_{min}}$ windows in a row, it is assumed that the minimum of the SiPM pulse is reached. The conditions are used to separate the small noise pulses from SiPM pulses. For the SensL 3x3 $\mathrm{mm}^2$ and the Hamamatsu 1x1 $\mathrm{mm}^2$ it is additionally demanded, that the voltage of the first sample in the last window in which the height $h_W$ was exceeded is smaller than $\boldsymbol{V_{min}}$. This is done because these two SiPMs have a low dark noise rate (see next chapters) and were connected to the laboratory board that features a constant baseline such that the smallest SiPM pulses could be differentiated from the baseline noise with this cut. The sample with the minimal voltage of the last window in which the height $h_W$ was exceeded is determined to be the minimum of the SiPM pulse. The maximum of the SiPM pulse is determined to be the sample with the maximal voltage in the first window in which the height $h_W$ was exceeded. If there is more than one maximum or minimum, respectively, the sample with the smaller time value is chosen. Time and voltage values of the maximum and the minimum sample are saved to a file. The procedure starts again with the first sample of the next window being the sample after the minimum of the SiPM pulse.
After all the recorded traces of an overvoltage are passed through, the time position of the pulse $\boldsymbol{t_{pulse}}$ and the pulse height $\boldsymbol{h_{pulse}}$ are determined. $t_{pulse}$ is chosen to be the time between the pulse minimum and maximum time $t_{min}$ and $t_{max}$, respectively, with $t_{pulse} = (t_{min} + t_{max})/2$. $h_{pulse}$ is chosen to be the difference between pulse minimum and maximum voltage.

**Additional cuts**
Now additional cuts can be applied to increase the signal to noise ratio and especially to cut pulses whose height is distorted.
As the pulse height of a SiPM pulse located on the rising edge of a previous pulse is decreased and therewith distorted, the time between two consecutive pulses, i.e. their pulse times $t_{pulse}$, has to amount to at least $\boldsymbol{t_{pulse}^{pulse}}$.
Furthermore pulses that are too close together to be distinguished are falsely identified as a single pulse. This false identification can be prevented with the choice of $h_W$. In figure 5.2 the two pulses in the middle of the picture are very close together such that the one pulse has just reached its maximum, when the other pulse stacks on top of it. If $h_W$ had been chosen too small, these two pulses would be identified as one pulse. Nevertheless, there are always some stacked pulses that are identified falsely as a single pulse. As they have a bigger temporal distance between their maximum and minimum sample than correctly identified pulses, pulses are cut if this temporal distance exceeds $\boldsymbol{t_{min}^{max}}$.

**Additional cuts for the ASCII board traces**
Two additional cuts were applied to the pulses extracted from the traces taken by the ASCII board. The SensL 6x6 $\mathrm{mm}^2$ SiPM has a high dark count rate because this SiPM is large and comprises considerably more G-APD cells as the other two SiPMs

(see table 3.1). Therefore many pulses superimpose on each other which distorts the pulse heights as described before. Only using pulses whose maximum sample, i.e. the baseline at which the falling edge of the pulse begins, sits above $\boldsymbol{V_{max_0}}$ was found out to cut several of these distorted pulses. The other additional cut for the ASCII board is used to improve the signal to noise ratio. This cut demands that the pulse height has to be at least $\boldsymbol{h_{pulse}^{min}}$ high.
All the algorithm variables and their typical sizes are summarized in table 5.1.

| **Variable** | **Typical size** | **Description** |
|---|---|---|
| $n_W$ | 10 | Amount of samples per window. |
| $h_W$ | 1 mV | Threshold: negative slope within window. |
| $n_{min}$ | 10 | Threshold: minimum amount of consecutive windows where $h_W$ is exceeded. |
| $V_{min}$ | 10 mV | Threshold: baseline noise removal (laboratory board only). |
| **Additional cuts** | | |
| $t_{pulse}^{pulse}$ | 300 ns | Threshold: minimum time between two consecutive pulses. |
| $t_{min}^{max}$ | 50 ns | Threshold: maximum time between pulse baseline and peak. |
| $V_{max_0}$ | -10 mV | Threshold: minimum baseline of a pulse (ASCII board only). |
| $h_{pulse}^{min}$ | 10 mV | Threshold: minimum pulse height (ASCII board only). |

**Table 5.1:** Overview of the algorithm variables and their typical sizes with short descriptions.

## 5.3 Spectrum fit functions

The pulse heights selected by the algorithm are filled into a histogram to obtain the finger spectrum. Two different fitting methods are used for the analysis of the finger spectrum. The fits are applied with the ROOT log-likelihood function.

**Gaussian fits**
One Gaussian function is fitted to the single p.e., the other to the 2 p.e. to determine the peak position of these two p.e.s. This is possible because the pulse heights are normally distributed around the position of the p.e.s if there is no systematic effect. The gain of the SiPM is determined to be the distance between the means of the two Gaussian functions. Moreover the error of the gain is calculated with the fit errors of the Gaussian means using a propagation of error. The crosstalk probability $p_{xt}$ is calculated as the ratio of pulse height entries above a threshold of 1.5 p.e. $N_{>1.5}$ and the total amount of entries in the finger spectrum $N$:

$$p_{xt} = \frac{N_{>1.5}}{N} \pm \frac{1}{N}\sqrt{N \cdot p_{xt}(1-p_{xt})}\ (stat.)\ . \tag{5.6}$$

Here the statistical error is chosen to be a binomial error as this error is used to estimate the frequency of groups within a histogram. A systematic error is estimated by setting the 1.5 p.e. threshold to values of 1.3 p.e. and 1.7 p.e., respectively. Here the 1.5 p.e. mark is determined from the mean values of the two Gaussian fits $G_{1pe}$ and $G_{2pe}$, with 1.5 p.e.=$(G_{1pe}$+$G_{2pe})/2$. The other p.e. marks are determined analogously.

**FACT spectrum fit**
The other fit function used in this analysis was developed by the FACT collaboration and uses a sum of Gaussian functions weighted with the modified Erlang distribution. Further information and the motivation of the FACT collaboration to use this fit function can be found in [26]. Hereafter, this fit function will be called "FACT spectrum fit".
The FACT spectrum fit is implemented as described in [26]:

$$f(x) = A_{1pe} \cdot \sigma_1 \cdot \sum_{n=1}^{N} \frac{e^{-\frac{1}{2}\left(\frac{x-x_n}{\sigma_n}\right)^2}}{\sigma_n} \cdot \frac{(n \cdot p_{fit} \cdot e^{-p_{fit}})^{n-1}}{((n-1)!)^{\nu}}\ . \tag{5.7}$$

The parameters of this fit function are given as follows. $A_{1pe}$ denotes the height of the single p.e. peak. $\sigma_n = \sqrt{n \cdot \sigma_{pe}^2 + \sigma_{el}^2}$ is the standard deviation of the nth p.e. peak and consists of the electronic noise and the noise of the nth p.e. peak. $x_n = n \cdot \text{gain} + x_0$ represents the position of the nth Gaussian mean which is shifted from the baseline by $x_0$. The sum walks through each of the in total $N$ Gaussian functions, such that $N$ is chosen to be the amount of fitted p.e.s plus one for each fitted finger spectrum, to make the fitting procedure more efficient. The first part of the sum are the Gaussian functions that depend on each other via the gain and $x_0$. The second part of the sum is the modified Erlang distribution with the Erlang exponent $\nu$. The modified Erlang distribution is needed to weight the nth Gaussian

function with the probability that n cell breakdowns occur [26].
A simulation presented in the FACT paper [26] connects the parameter $p_{fit}$ with the crosstalk $p_{xt}$. Thereto it is assumed that only directly neighbouring cells contribute to the crosstalk. The result of this simulation is used in this analysis to obtain the crosstalk probability:

$$p_{xt} = 0.723(4) \cdot \left( \frac{p_{fit}}{0.440106(100)} \right)^{\frac{0.875(5)}{0.9515(20)}} \tag{5.8}$$

To estimate the statistical error on $p_{xt}$, the fit error of $p_{fit}$ is used with a propagation of error. The systematic error caused by the simulation parameters is estimated from variations of the parameters by their given errors. The largest achieved deviation from $p_{xt}$ is chosen to be the systematic error.
The gain and its error are obtained through the corresponding fit parameter.

## 5.4 SensL 3x3 mm$^2$ SiPM with laboratory board

At first the preliminary measurement of the breakdown voltage is to be analysed. The interval within which the SiPM pulses disappeared was restricted to bias voltages between 24.80 V and 24.90 V. Estimating the error with respect to the width of the interval and the error on the displayed bias voltage of the EA-PSI 6150-01 DC power supply, the breakdown voltage is determined at $T_{SiPM} = (22.0 \pm 0.3\ (\text{stat.}) \pm 0.5\ (\text{syst.}))\,°\text{C}$:

$$V_{Bd} = (24.850 \pm 0.040)\text{V} \ . \tag{5.9}$$

For this SiPM, traces were only recorded for the bias voltage of $(29.850 \pm 0.015)$ V. This error is again estimated and quadratically added with the error of the breakdown voltage to obtain the error on the overvoltage of $(5.000 \pm 0.043)$ V.
To set the variables for the extraction algorithm properly, single pulses of a recorded trace are examined. As one can see in figure 5.2 or even in the oscilloscope screenshot of the SiPM chapter in figure 3.3, the single p.e. SiPM pulses are about 200 ns long and roughly 30 mV high. While the baseline does not fall under 0.007 V, the minima of the single p.e.s are located under -0.01 V. The steeply falling edge of the SiPM pulses comprises roughly 15 samples. After training the algorithm variables on the derived finger spectra, the values in table 5.2 are chosen.

| $n_W$ | $h_W$ | $n_{min}$ | $V_{min}$ | $t_{pulse}^{pulse}$ | $t_{min}^{max}$ |
|---|---|---|---|---|---|
| 6 | 3 mV | 5 | 5 mV | 250 ns | 50 ns |

**Table 5.2:** The chosen algorithm variables for the SensL 3x3 mm$^2$ SiPM.

An extract of a recorded trace at $V_{Ov}$=5.000 V is shown in figure 5.3. Here the additional cuts ($t_{pulse}^{pulse}$ and $t_{min}^{max}$) were not performed and the extracted minimum and maximum samples are marked with blue triangles. The baseline is constant and the majority of the pulses are single p.e.s as it is typical for a dark noise measurement. The SiPM pulses seldomly stack onto each other. The large pulse at the left of the figure is truncated as it leaves the vertical full range (-0.14 V) of the oscilloscope. On the one hand no pulses are extracted in the electronic noise on the other hand all the recognizable SiPM pulses are identified. Therefore the pulse extraction algorithm seems to work as desired.
A discrete Fourier transform using the Python package numpy was performed for an entire SiPM trace as shown in figure 5.4. A possible reason for the peak at about 100 MHz are the falling edges of the SiPM pulses. These falling edges have an infinite slope, i.e. an infinite frequency response, for an ideal SiPM. The gain constellation of the transimpedance amplifier used on the laboratory board decreases the slope of the falling edge of the SiPM pulses as it has a finite bandwidth. A SPICE simulation encourages the assumption that this causes the peak at 100 MHz. This peak structure is also located in the DFTs of the Hamamatsu SiPM traces which were taken with the same laboratory board. For the ASCII board, the peak is shifted to about 50 MHz which is possibly explainable with the integrated preamplifier.

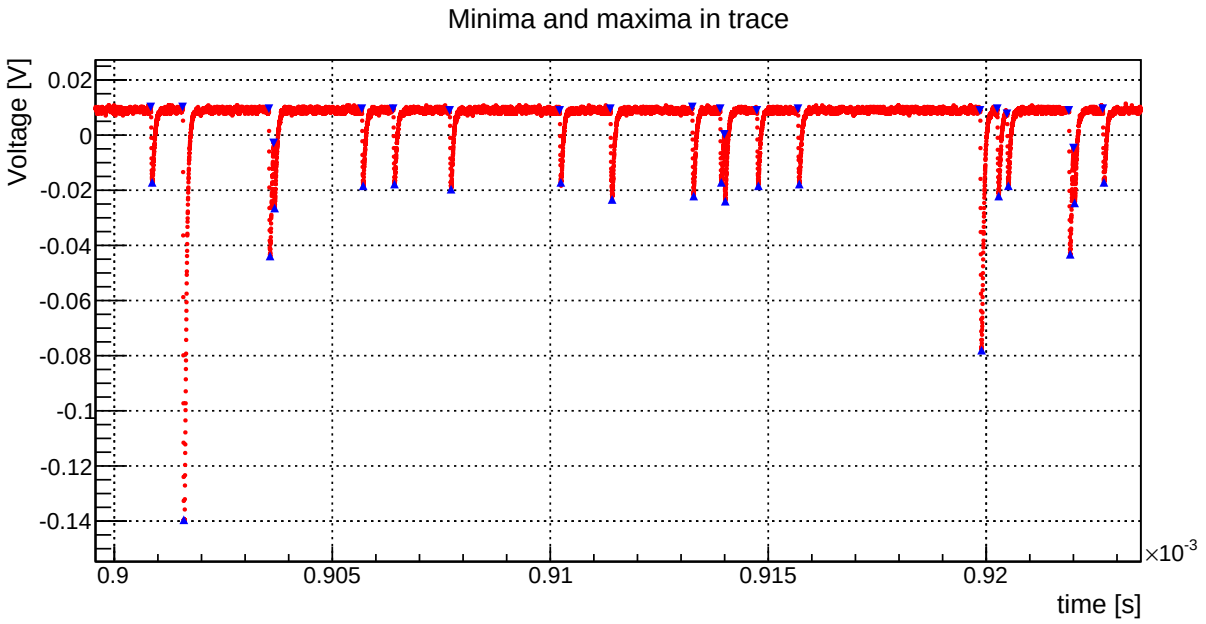


**Figure 5.3:** Extract of a SensL 3x3 mm$^2$ SiPM trace taken by the laboratory board at $V_{Ov}$=5.000 V. The small blue triangles mark extracted pulse minima and maxima. The pulses in the middle of the figure are single p.e.s. Here the additional cuts were not used.

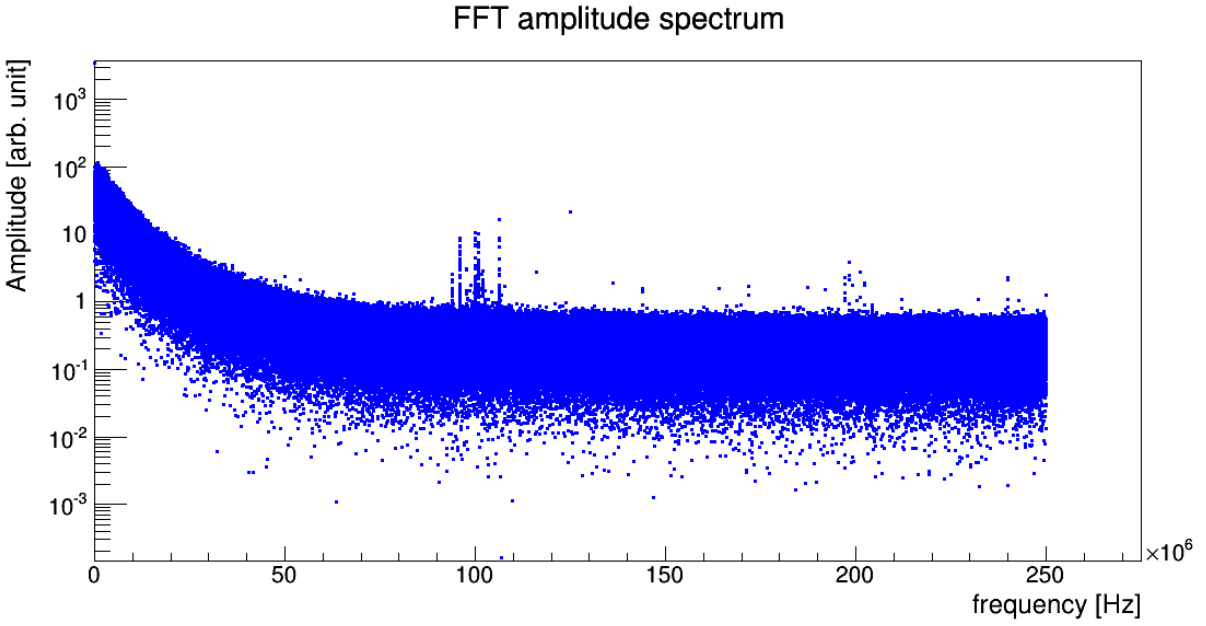


**Figure 5.4:** Discrete Fourier transform amplitude spectrum of an entire SensL 3x3 mm$^2$ SiPM trace at $V_{Ov}$=5.000 V. A possible reason for the peak at about 100 MHz is given in the text.

The finger spectra in figure 5.5 are obtained with the above stated algorithm variables. Here and in the following the errors on the bin heights are Poisson errors $\sqrt{N}$,

with $N$ being the amount of entries within the bin.
The first and highest peak at the left side corresponds to the single p.e. and is fitted with the blue lined Gaussian function. Because of the peak asymmetry the FACT spectrum fit is not used here. The Gaussian functions are used as they serve as a weighted mean to find the peak maximum. Moreover the crosstalk is calculated via the derived 1.5 p.e. mark and the raw data such that the height of the Gaussian function does not influence the crosstalk as it is the case for the FACT spectrum fit. In the upper half of the figure, the additional cuts are not used such that pulses stacked onto a previous pulse are taken into account. This leads to the widened left flanks of the p.e.s. At the left side of the single p.e. there is a plateau that is caused by afterpulses as it is found out that the pulses of this plateau region always appear shortly after a previous SiPM pulse. Therefore, this plateau as well as the left widened flanks of all the p.e.s are cut with the additional cuts as it is to be seen in the lower half of the figure. Nevertheless, the cuts do not affect the plateaus at the right side of each p.e.
These plateaus are considered more detailed as they seem to have a systematic background. A zoom into a SiPM trace that is used to extract pulses for the finger spectrum is shown in figure 5.6. All the three pulses are single p.e.s. The outer pulses, whose maxima and minima are marked with blue triangles, are pulses from the plateau region on the right side of the single p.e. Obviously the pulse heights are extracted correctly by the algorithm such that the plateau is no artefact of the algorithm. Possible explanations are the SensL SiPM itself or the synergy of the laboratory board and the SensL SiPM. That these plateaus are caused by the laboratory board solely is not assumed as they do not appear in the finger spectrum of the Hamamatsu SiPM, shown in figure 5.7 of the next chapter.
Gain and crosstalk are calculated for both finger spectra which is shown in the legend of figure 5.5. For the finger spectrum derived from the algorithm with applied additional cuts the gain equals $(27.214 \pm 0.052)\,\mathrm{mV}$ and the crosstalk $p_{xt}$ for the applied overvoltage of $V_{Ov} = (5.000 \pm 0.043)\,\mathrm{V}$ is given as:

$$p_{xt} = 0.2138 \pm 0.0029\ (stat.) \pm 0.001(syst.).$$

The crosstalk for the SensL 3x3 mm$^2$ SiPM is stated to be 7% for an overvoltage of 2.5 V in the datasheet of the SensL C-Series (see table 3.1). As the overvoltage is not equal to the one used in this thesis, a comparison is not performed. Instead, the datasheet of the SensL J-Series SiPMs [27] is used. As the crosstalk at an overvoltage of 2.5 V is given with 7.5% for the J-Series 3x3 mm$^2$ SiPM with 35 $\mu$m cell size [27], this SiPM can be compared with the SensL C-Series SiPM used in this thesis. The crosstalk of the J-Series SiPM is stated to be 20% at an overvoltage of 5 V [27]. Therefore the crosstalk determined in this analysis is compatible with the literature value as the error on $p_{xt}$ stated above does not include the error on the overvoltage.

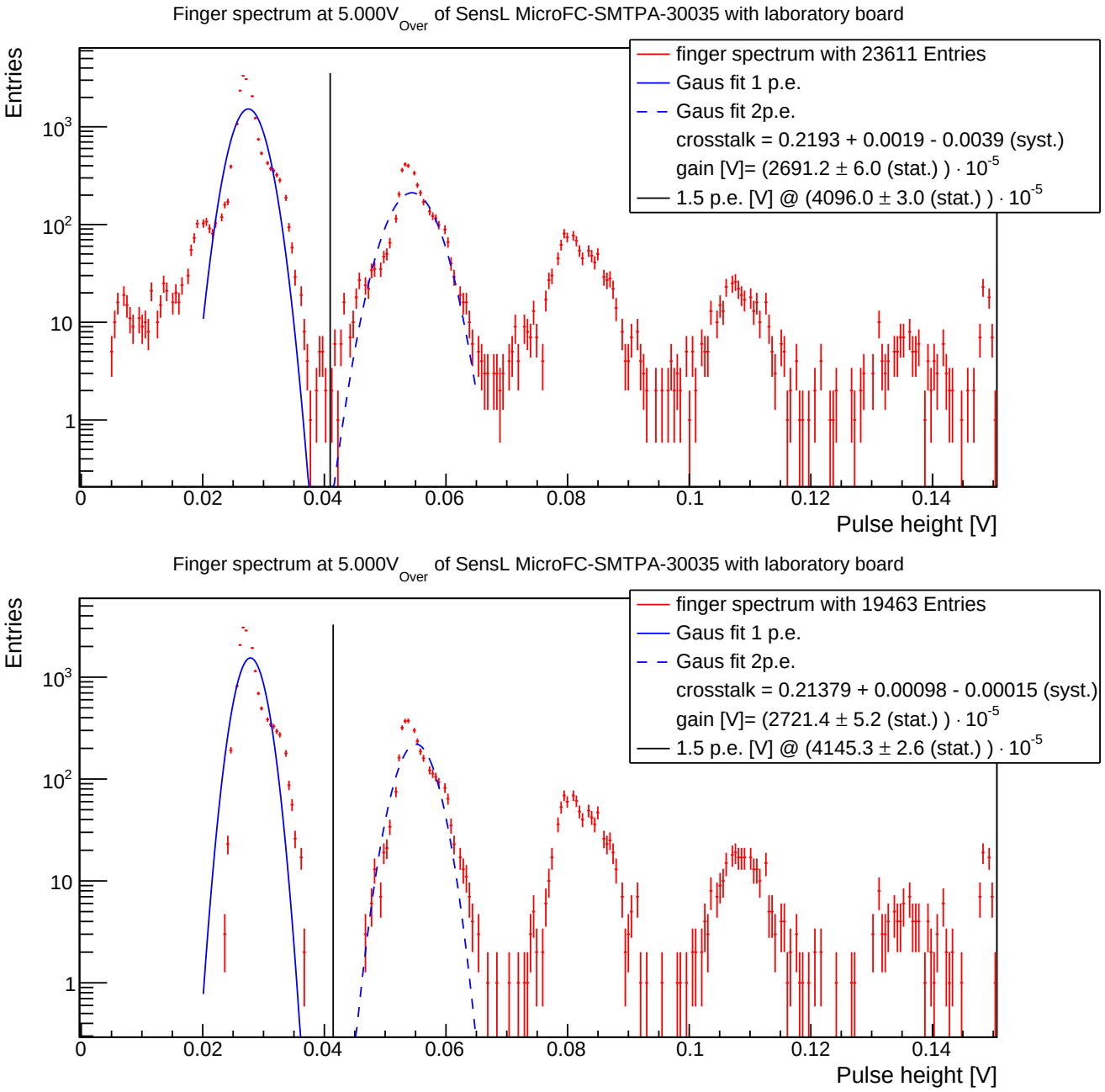


**Figure 5.5:** Finger spectra of SensL 3x3 mm$^2$ SiPM at $V_{Ov} = 5.000\,\mathrm{V}$ without additional cuts at the top and with additional cuts at the bottom. Two Gaussian functions are used to determine the gain and the 1.5 p.e. mark which is used to calculate the crosstalk. The first peak on the left (highest peak) is the single p.e. Even with the additional cuts, there are plateaus on the right of each p.e. peak.

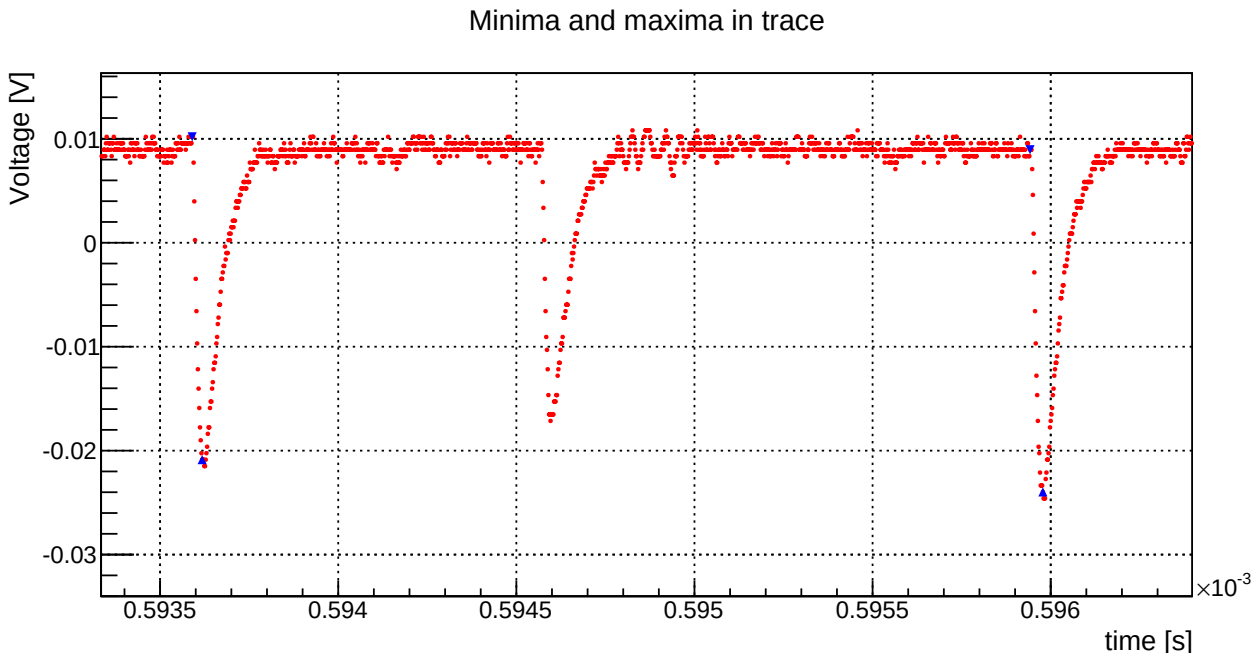


**Figure 5.6:** Zoom into a recorded SensL 3x3 mm$^2$ SiPM trace taken by the laboratory board at $V_{Ov}$=5.000 V. The small blue triangles mark extracted pulse minima and maxima of the plateau region on the right side of the single p.e. The pulse in the middle of the figure is a single p.e., too.

## 5.5 Hamamatsu 1x1 mm$^2$ SiPM with laboratory board

The preliminary measurement of the breakdown voltage of the Hamamatsu 1x1 mm$^2$ SiPM at $T_{SiPM} = (22.37 \pm 0.11\ (\text{stat.}) \pm 0.15\ (\text{syst. } V_{\text{ref}}))\,^\circ\text{C}$ yields:

$$V_{Bd} = (64.27 \pm 0.03)\,\text{V}\ . \tag{5.10}$$

SiPM traces are measured and analysed for bias voltages of $(64.87 \pm 0.01)$ V and $(65.67 \pm 0.01)$ V. This yields overvoltages of $(0.60 \pm 0.03)$ V and $(1.40 \pm 0.03)$ V. After some training of the algorithm on the recorded traces, the variables of the algorithm are chosen as stated in table 5.3. It was taken into account, that the Hamamatsu SiPM features pulses that have steeper falling and rising edges than the pulses of the SensL SiPMs. Here the rising edge of a SiPM pulse denotes the signal during the recharge of a G-APD. Furthermore the $V_{min}$ cut has to be changed to $V_{min} = 10$ mV for the smaller overvoltage of 0.60 V because the single p.e.s do not reach under $V_{min} = 5$ mV as they do at an overvoltage of 1.40 V.

| $n_W$ | $h_W$ | $n_{min}$ | $V_{min}$ | $t_{pulse}^{pulse}$ | $t_{min}^{max}$ |
|---|---|---|---|---|---|
| 4 | 1 mV | 3 | 5 mV* | 250 ns | 30 ns |

**Table 5.3:** The chosen algorithm variables for both overvoltages. The given $V_{min}$ value is only used for the overvoltage of 1.40 V. $V_{min}$=10 mV has to be chosen for the overvoltage of 0.60 V.

The finger spectrum for the overvoltage of 1.40 V is shown in figure 5.7. Here the additional cuts of the algorithm are applied. The SiPM pulses of 60 SiPM traces, each of a length of 1 ms, are filled into this finger spectrum. As there are only about 7000 entries, the dark noise rate of this SiPM is very low compared to the SensL 3x3 mm$^2$ SiPM, for whom only half as many traces were analysed to obtain about 3 times more entries. Therefore the p.e. peaks are perfectly separated such that the systematic error on the crosstalk is zero because there are no entries between the 1.3 p.e. and the 1.7 p.e. mark. Furthermore, there are no plateaus at the right of the p.e.s as with the previously analysed SensL SiPM.
The algorithm is also applied to the recorded traces of the 0.60 V overvoltage and the additional cuts are used again. Gain and crosstalk values are derived from the two Gaussian fits and the 1.5 p.e. mark for both overvoltages. The results are stated in table 5.4. The error on the determined crosstalk is the binomial error. There are listed literature values for the crosstalk, too. The literature values are derived from the paper [28]. In this paper, the measured crosstalk probabilities are plotted against the temperature corrected gain and a function is fitted to the data. This function is used in this thesis to calculate the crosstalk for the two given overvoltages. Moreover the crosstalk was estimated from a crosstalk against overvoltage plot in the Hamamatsu datasheet [9].

| $V_{Ov}$ [V] | Gain [mV] | $p_{xt}$ | Literature $p_{xt}$ | Datasheet $p_{xt}$ |
|---|---|---|---|---|
| 1.40 ± 0.03 | 20.092 ± 0.029 | 0.3376 ± 0.0056 | 0.3751 | 0.35 |
| 0.60 ± 0.03 | 9.112 ± 0.080 | 0.0947 ± 0.0050 | 0.1216 | 0.06 |

**Table 5.4:** This table contains the results of the gain and crosstalk determination for the Hamamatsu 1x1 mm² SiPM. Additionally literature [28] and datasheet [9] values are stated for the crosstalk.

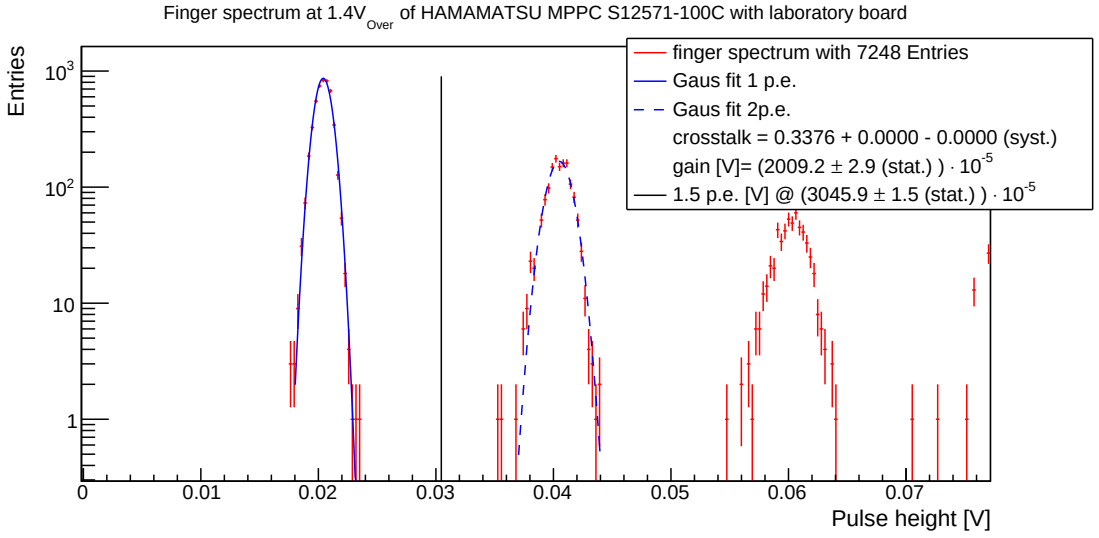


**Figure 5.7:** Finger spectrum of Hamamatsu 1x1 mm² SiPM at an overvoltage of $V_{Ov}$=1.40 V. The additional cuts of the algorithm are applied. The left peak correspondes to the single p.e. As there are no entries between the 1.3 p.e. and 1.7 p.e. mark, the calculated systematic error on the crosstalk $p_{xt}$ equals zero. The legend box covers some bins at the right margin of the finger spectrum.

Once again the error on the crosstalk does not include the error on the overvoltage. The errors on the literature and datasheet value are not given and the deviation of the literature values from the datasheet is not discussed in the paper [28]. Therefore the crosstalk probabilities, that are determined in this analysis, are assumed to be compatible with the literature and the datasheet values as they differ by only a few sigmas even without considering the error on the overvoltage.
The determined gain values are plotted against the bias voltage of the SiPM to determine the breakdown voltage via a linear regression. This yields a breakdown voltage of:

$$V_{Bd} = (64.21 \pm 1.71)\,\mathrm{V}.$$

As only two gain values are determined, the error is larger than the one of the preliminary measurement of the breakdown voltage. Even within the scope of the error of the preliminary determined breakdown voltage (see equation (5.10)), the two values are within a 3-$\sigma$ scope which is a adequate result.

## 5.6 Main measurement with SensL 6x6 mm$^2$ SiPM and ASCII board

The preliminary breakdown voltage measurement of the SensL 6x6 mm$^2$ SiPM at a temperature of $T_{SiPM} = (22.32 \pm 0.11\ (\text{stat.}) \pm 0.15\ (\text{syst. } V_{\text{ref}}))\,°\text{C}$ yields:

$$V_{Bd} = (24.65 \pm 0.10)\,\text{V} \ . \tag{5.11}$$

The estimated error is larger than for the SiPMs on the laboratory boards as the linear regulator between the Voltcraft power supply and the SiPM decreases the step size that can be used to set the bias voltage of the SiPM which is described in chapter 4.2.
SiPM traces were recorded for four different overvoltages. The chosen overvoltages and the bias voltages that had to be applied to the SiPM to achieve the different overvoltages are given in table 5.5. The errors on the bias voltage are all estimated to be 0.01 V. To obtain the errors on the overvoltages, which are always 0.10 V, the error of the corresponding bias voltage is quadratically added with the error on the breakdown voltage.

| | | | | |
|---|---|---|---|---|
| $V_{bias}$ [V] $\pm$ 0.01 V | 28.50 | 28.87 | 29.47 | 29.85 |
| $V_{Ov}$ [V] $\pm$ 0.10 V | 3.85 | 4.22 | 4.82 | 5.20 |

**Table 5.5:** The four applied bias voltages with the corresponding overvoltages.

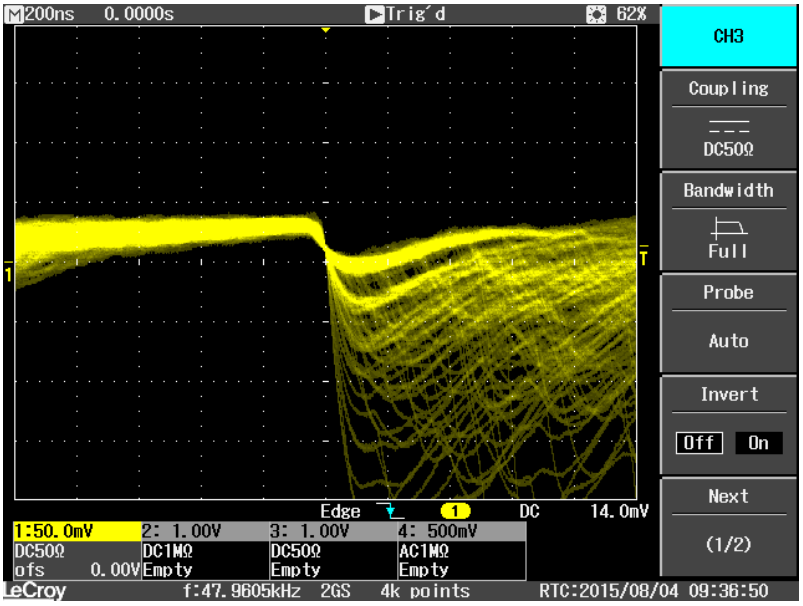


**Figure 5.8:** Dark noise signal of SensL 6x6 mm$^2$ SiPM processed and amplified by the ASCII board. The screenshot is taken by the LeCroy WaveJet 354A. Voltage (div=50 mV) is plotted against time (div=200 ns).

An oscilloscope screenshot at the overvoltage of $V_{Ov} = 5.20$ V is shown in figure 5.8. The SiPM is placed in darkness and the threshold is set to about 0.5 p.e in a falling

edge mode. The first three p.e.s can be distinguished though the dark noise is so high that the pulses stack onto each other. The single p.e. has a height of about 30 mV and the pulses are roughly 500 ns long. By zooming into a trace and focussing on a single pulse, it is found out that the falling edge of the SiPM pulses is flatter than for the previously analysed SiPMs. It comprises roughly 40 samples. As the sampling rate amounts to 250MSps, this is equal to 160 ns. All this information is used to chose the algorithm variables properly. Moreover the algorithm is trained on the traces of the highest overvoltage $V_{Ov} = 5.20$ V. The resulting choice of the algorithm variables is shown in table 5.6.

| $n_W$ | $h_W$ | $n_{min}$ | $t_{pulse}^{pulse}$ | $t_{min}^{max}$ | $V_{max_0}$ | $h_{pulse}^{min}$ |
|---|---|---|---|---|---|---|
| 14 | 0 mV | 17 | 400 ns | 230 ns | -10 mV | 14 mV |

**Table 5.6:** The chosen algorithm variables that are used for all overvoltages.

A zoomed trace taken at the overvoltage $V_{Ov} = 5.20$ V is shown in figure 5.9. The blue triangles mark the pulse minima and maxima that are extracted by the algorithm without using the additional cuts. As expected, the dark count rate of this large SensL SiPM is considerably higher than the one of the SensL 3x3 mm$^2$ (see figure 5.3). Due to the high dark noise rate, there is no constant baseline. As the pulses stack onto each other, the p.e. peaks of the extracted finger spectrum are expected to merge into each other.

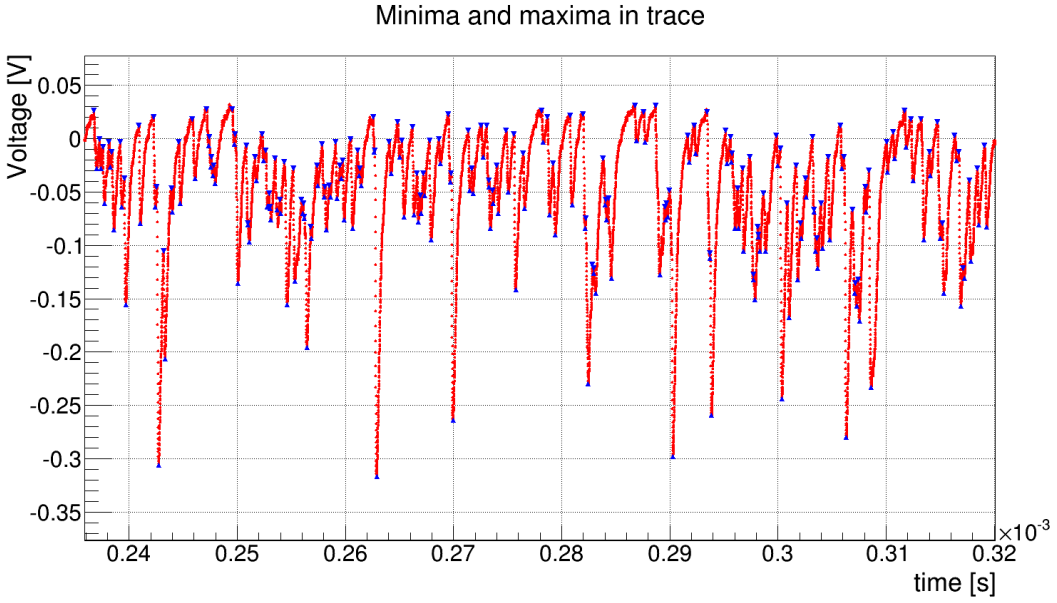


**Figure 5.9:** Zoom into a recorded SensL 6x6 mm$^2$ SiPM trace taken by the ASCII board at $V_{Ov}$=5.20 V. The small blue triangles mark the pulse minima and maxima that are extracted by the algorithm without using the additional cuts. Obviously the dark noise rate is higher than in figure 5.3 of the SensL 3x3 mm$^2$ SiPM.

The finger spectra for $V_{Ov} = 5.20$ V without and with the additional cuts are shown in the upper and lower part of figure 5.10. As expected, the p.e. peaks merge into

each other without using additional cuts. Whereas the application of these cuts leads to the desired finger form. The FACT spectrum fit was chosen instead of the Gaussian fits, as it takes into account more than only two p.e.s and does not fit the p.e.s independently. The fit is not performed above a pulse height of 0.3 V as pulses reaching the full range of the oscilloscope bias the data from there on.

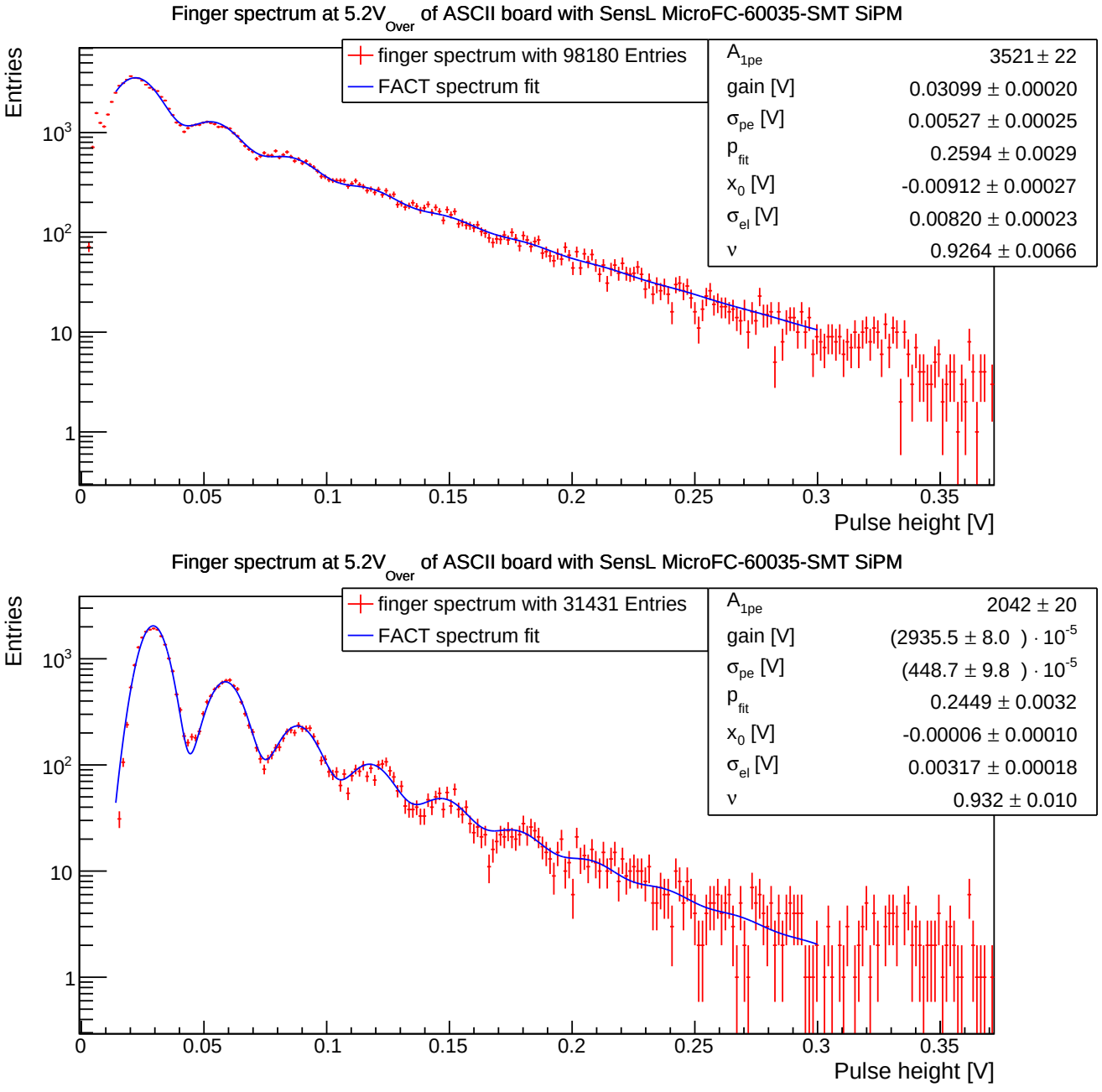


**Figure 5.10:** Finger spectra of the SensL 6x6 mm$^2$ SiPM at $V_{Ov} = 5.20$ V without additional cuts at the top and with additional cuts at the bottom. The first peak on the left is the single p.e. The additional cuts increase the separation between the p.e. peaks.

The algorithm is applied to the traces of all overvoltages and the additional cuts are used to obtain a more reliable gain value. The crosstalk probabilities (see equation (5.8) in chapter 5.3) and gain values are shown in table 5.7.

| $V_{Ov}$ [V] ± 0.10 V | $p_{xt}$ | Gain [mV] |
|---|---|---|
| 3.85 | 0.3013 ± 0.0036 (stat.) ± 0.0038 (syst.) | 21.001 ± 0.066 (stat.) |
| 4.22 | 0.3357 ± 0.0039 (stat.) ± 0.0040 (syst.) | 23.186 ± 0.086 (stat.) |
| 4.82 | 0.3913 ± 0.0045 (stat.) ± 0.0041 (syst.) | 27.250 ± 0.065 (stat.) |
| 5.20 | 0.4217 ± 0.0050 (stat.) ± 0.0042 (syst.) | 29.355 ± 0.080 (stat.) |

**Table 5.7:** This table contains the results of the gain and crosstalk determination for the SensL 6x6 mm$^2$ SiPM connected to the ASCII board.

The crosstalk probabilities are large compared to the 7% at an overvoltage of 2.5 V stated by the manufacturer. There were no literature values found that might confirm or falsify these high values. Nevertheless it is assumed that the crosstalk probabilities are determined correctly by the algorithm, as they were compatible to the literature values for the other SiPMs analysed before. For the finger spectrum of the traces recorded at an overvoltage of 5.2 V the fit consisting of two Gaussian functions was applied, too. A significant deviation of gain and crosstalk from the FACT spectrum fit results was not found. The SiPM of an ASCII module is optically coupled with plexiglass. This coupling is also chosen for the SiPMs at FACT and decreases the crosstalk which is stated in a FACT publication. A possible reason is the influence of the refraction index of plexiglass that is higher than the one of air and changes the angle of total reflection, such that crosstalk photons can leave the SiPM instead of being refracted and generating a crosstalk event.
As a cross-check of the breakdown voltage, the linear dependence of the gain on the overvoltage is used like for the Hamamatsu SiPM. A ROOT $\chi^2$-fit is performed on the four data points as shown in figure 5.11. The $\chi^2$/(ndf) of about 3 and the residual graph yield that the errors on gain and bias voltage are estimated a bit too small. Moreover, gain measurements at lower bias voltages are needed to determine the breakdown voltage more exactly. The resulting breakdown voltage of $(25.17 \pm 0.56)$ V is located within a 1-$\sigma$ interval above the preliminary measured breakdown voltage. This indicates that the breakdown voltage was determined correctly before.

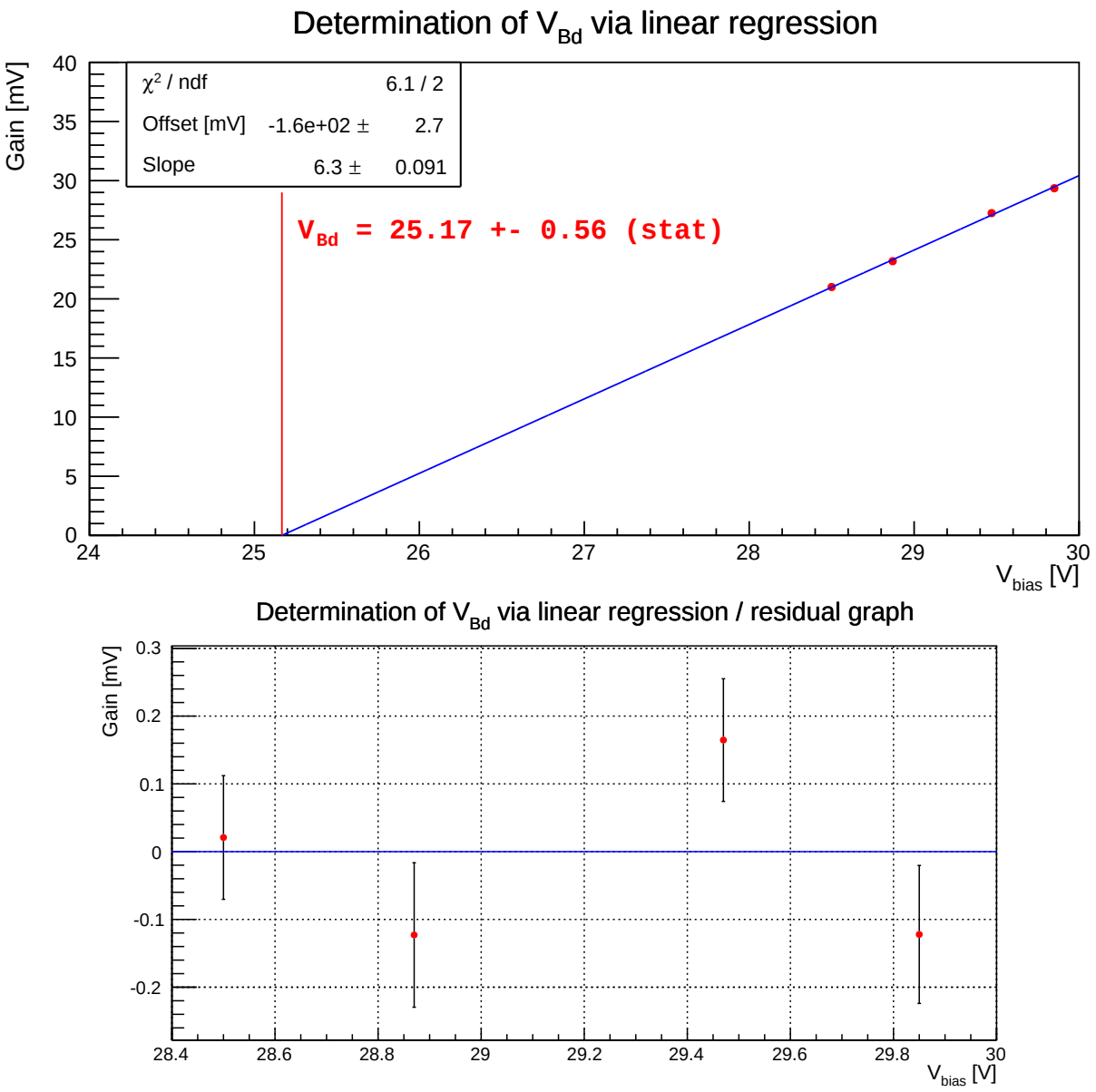


**Figure 5.11:** In the upper half the determination of the breakdown voltage via a linear regression is shown. In the lower half the associated residual graph is shown.

### 5.6.1 Simulation of the UB algorithm

The UB algorithm is implemented and applied to the recorded dark noise traces processed by the ASCII board used in this thesis. This is done to compare the result with the results from the ASCII modules that are operated at the Pierre Auger Observatory and house a SiPM and a ASCII board manufactured at the RWTH Aachen University.
Minimum ionizing particles (MIPs) of an extensive air shower are detected by the PMTs in the water Cherenkov tanks of the SD. The UB algorithm triggers on these and integrates the charge from 3 samples before the trigger signal appears until 16 samples after it. But the ASCII module only detects a signal with a probability of

about 15% as it does not cover the whole surface of the SD tank. Therefore the UB trigger is a random trigger in 85% of the cases [6]. As stated at the end of chapter 2, the sampling rate of the UB amounts to 40MSps. Therefore the performed integral of 20 samples is spread over 500 ns. Figure 5.12 shows an example of a charge spectrum that is generated by applying the UB algorithm on the data that is recorded at the Pierre Auger Observatory by ASCII modules that house an SiPM and a ASCII board manufactured at the RWTH Aachen University. It does not feature a single p.e. resolution but the change of the slope and the little bump in the spectrum might be caused by the MIP events that are triggered by the PMTs of the SD.
The question is, if it is possible to derive a single p.e. resolution from the measured dark noise traces of this thesis by applying the UB algorithm as thereby the required gain can be determined.

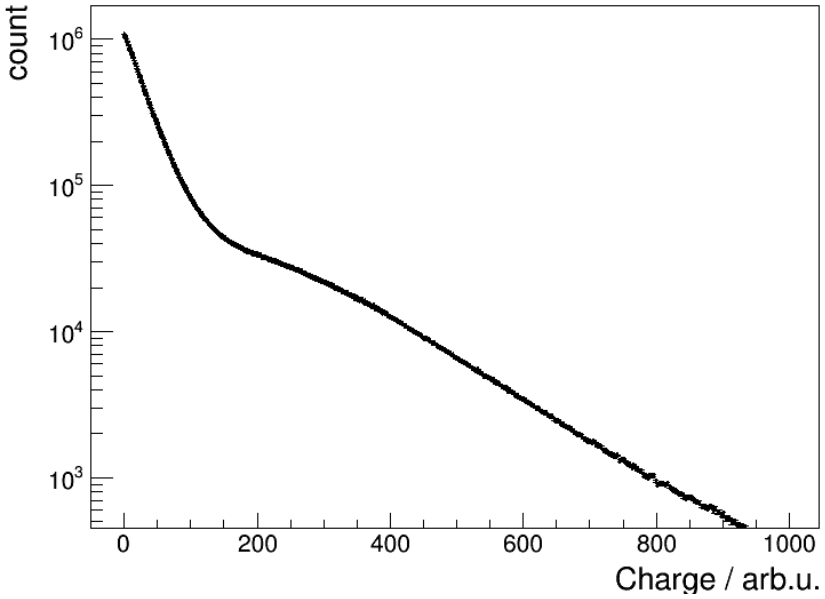


**Figure 5.12:** Charge spectrum derived from the UB algorithm at the Pierre Auger Observatory. The steeply falling edge on the left side of the spectrum are dark noise events. The knee and the little bump in the spectrum might be caused by MIPs.

A software-based low-pass filter with a cutoff frequency of 20 MHz is needed to simulate the UB low-pass filter. In order to do this a type I Chebyshev filter of 18th order is used. This filter is provided by the Python package scipy.signal. Other filters were tested, but the Chebyshev filter was the most efficient one. After applying the filter, the sampling rate of 250 MSps has to be decreased to 40 MSps. The position of a new sample is approximated via a linear interpolation between the two next neighbouring old samples.
Now a self-developed algorithm is applied to the SiPM traces with an overvoltage of $V_{Ov} = 4.82\,\mathrm{V}$.
There are not any MIP signals in the SiPM traces of this thesis such that not only 85% but 100% of the triggers are chosen to be random. As the trigger is random,

the integration can be shifted such that the integral is performed from the sample at which the trigger occurs until 19 samples later. For reasons of efficiency and simplification the position of a generated random sample and the corresponding integration intervals are not saved, though this would prevent the algorithm from triggering more than once in a particular interval. Instead, only 10% of each trace are randomly integrated to reduce this probability. A spot test for a single trace revealed, that only very few intervals overlapped such that this method is used.
The resulting charge spectrum is shown in figure 5.13. Obviously there does not exist a single p.e. resolution. Therefore a gain determination of the SiPM is not possible.
Probably, the high dark noise of the 6x6 $mm^2$ SiPM causes this low resolution on the single p.e. basis. Therefore test measurements with the ASCII board and a smaller SiPM, like the SensL 3x3 $mm^2$ SiPM used in this thesis, can be performed in the future to find out if the UB algorithm works better with SiPMs having a lower dark noise. Moreover the UB algorithm itself reduces the resolution on the single p.e. basis as the algorithm that is developed in this thesis is able to separate the p.e. peaks such that the gain of the SiPM can be determined.

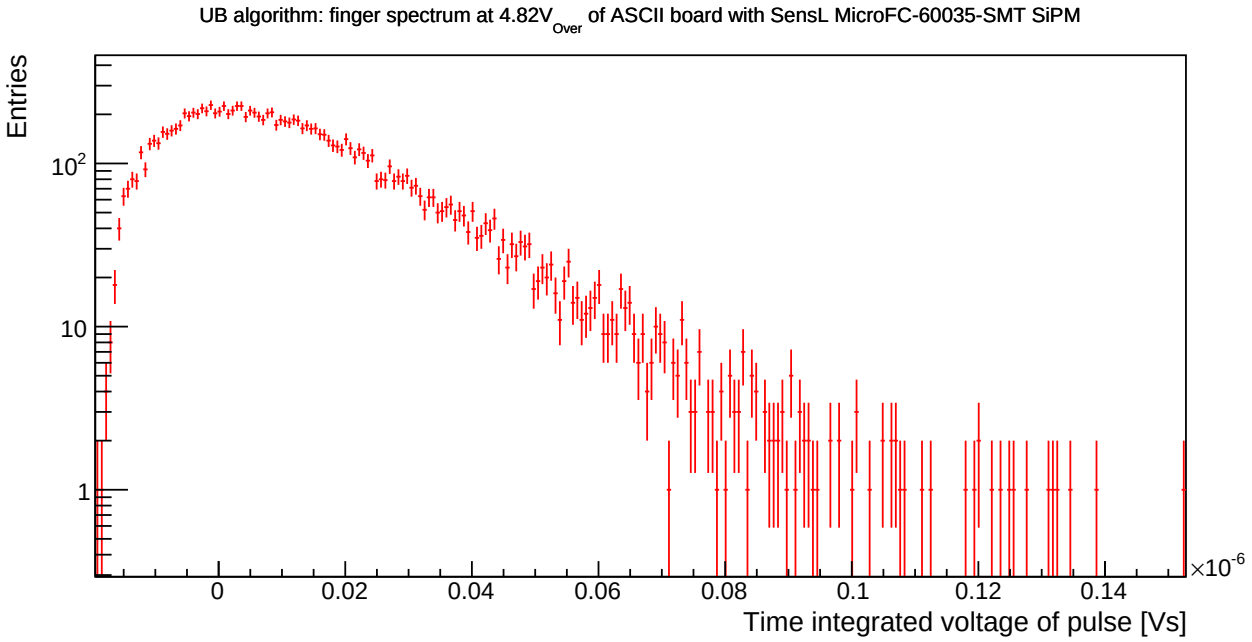


**Figure 5.13:** Charge spectrum with 12000 entries derived from the simulated UB algorithm on the dark noise traces of the SensL 6x6 $mm^2$ SiPM. The overvoltage amounts to $V_{Ov} = 4.82\,V$. The p.e. peaks are merged together and cannot be seen.

# 6. Conclusion and Outlook

The Pierre Auger Observatory is currently upgraded for a further improvement of the measurement of extensive air showers (EASs) generated by ultra-high-energy cosmic rays (UHECRs). The muonic component of an EAS can be used to investigate the mass composition and the energy of UHECRs. Therefore the upgrade comprises among others the scintillating surface detector (SSD) to improve the distinction of the electromagnetic and the muonic component of an EAS. A prototype of the SSD is the ASCII detector. Some of the ASCII modules are not operated with photomultiplier tubes (PMTs) but with silicon photomultipliers (SiPMs) as it was proposed by the III. Phys. Inst. of the RWTH Aachen University. The SiPM of an ASCII module is connected to the ASCII board that was developed and manufactured at the RWTH Aachen University. One advantage of SiPMs compared to PMTs is the possibility to measure their gain using their finger spectrum which improves the understanding of changes of the gain of the whole detector.

In this thesis an algorithm was developed that extracts single SiPM pulses from SiPM traces to obtain a finger spectrum and determine the gain of the SiPM among others. The algorithm had been tested on two SiPMs that are each connected to a laboratory board, before it was applied to the SiPM connected to the ASCII board currently installed in some ASCII modules of the Pierre Auger Observatory.
Finger spectra with a single p.e. resolution could be created for all SiPM dark noise traces by using the developed algorithm. Even for the traces of the SiPM on the ASCII board, which suffered from a high dark noise rate and imperfect electronics, the p.e. peaks of the created finger spectra were clearly distinguishable. This was achieved as the algorithm searches for SiPM pulses and determines their height, instead of integrating the charge of SiPM pulses which is biased by the stacking of SiPM pulses. Moreover the sensitivity of the algorithm was increased by using cuts. Therefore the algorithm can be used successfully even for large SiPMs with a high dark noise rate and corresponding high probability for stacking of pulses. Furthermore for all SiPMs the crosstalk probability could be determined from the finger spectra. The derived values were compatible with the literature values. Moreover the gain could be determined from the finger spectra.
Finally the UB algorithm was implemented using a random trigger and integrating the charge for a specific time. The application to the dark noise traces of the SiPM on the ASCII board lead to a finger spectrum that does not feature a single p.e. resolution, such that the gain was not determinable.

Therefore the self-developed algorithm is better than the UB algorithm and can be used to determine the gain of the SiPMs used in some ASCII modules at the Pierre Auger Observatory.

To be able to determine the algorithm variables automatically a function can be added to the algorithm in the future to extract the variables from a small part of the trace. All in all the developed algorithm is easy to be implemented and can be used to derive a finger spectrum with a single p.e. resolution from SiPM traces. Furthermore gain and crosstalk can be determined for SiPMs at several detectors using SiPMs as for instance the ASCII detector.

# References


[1] Pierre Auger Collaboration, *The Pierre Auger Observatory Upgrade Preliminary Design Report (internal)*. Available online http://auger.fnal.gov/upgrade_review/, visited 09.05.2015, Apr. 2015.

[2] J. Blümer, R. Engel, and J. R. Hörandel, *Cosmic Rays from the Knee to the Highest Energies*, Progress in Particle and Nuclear Physics, 63 (2009), pp. 293–338. Available online http://www.sciencedirect.com/science/article/pii/S0146641009000362, visited 09.03.2015.

[3] M. Rao and B. Sreekantan, *Extensive Air Showers*, World Scientific Publishing Co. Pte. Ltd., 1998. ISBN 981-02-2888-0.

[4] O. Pooth, *Experimentalphysik V Einführung in die Teilchen- und Astroteilchenphysik*. Jan. 2013.

[5] A. Aab *et al.*, *The Pierre Auger Cosmic Ray Observatory*, Nuclear Instruments and Methods in Physics Research A, 798 (2015), pp. 172–213. Available online http://www.sciencedirect.com/science/article/pii/S0168900215008086, visited 09.03.2015.

[6] *Private communication with X. Bertou, Centro Atómico Bariloche, 2015.*

[7] D. Renker and E. Lorenz, *Advances in solid state photon detectors*, 2009 JINST 4 P04004. Available online http://iopscience.iop.org/article/10.1088/1748-0221/4/04/P04004/pdf, visited 09.05.2015.

[8] SensL, *C-Series Datasheet Rev. 1.9, Preliminary*, Aug. 2015. Available online http://www.sensl.com/downloads/ds/DS-MicroCseries.pdf, visited 08.29.15.

[9] Hamamatsu, *MPPC S12571 series Datasheet*, Oct. 2013. Available online http://www.hamamatsu.su/images/hamam/Tech/S/s12571-025_etc_kapd1042e03.pdf, visited 08.29.15.

[10] *LibLAB project website*. https://forge.physik.rwth-aachen.de/projects/liblab, visited 09.11.15.

[11] J. Schumacher, *Front-end Electronics for Silicon Photomultipliers*, master's thesis, III. Phys. Inst. A, RWTH Aachen University, Jan. 2014.

[12] intersil, *Datasheet of EL5163,EL5165,EL5364*, Jan. 2014. Available online http://www.intersil.com/content/dam/Intersil/documents/el51/el5164-165-364.pdf, visited 09.07.15.

[13] EA (Elektro-Automatik), *Datasheet of EA-PSI 6000 Series.* Available online http://www.datatec.de/shop/artikelpdf/psi6032-06_1_d.pdf, visited 08.29.15.

[14] PeakTech, *Operation manual*, Jul. 2013. Available online http://www.peaktech.de/productdetail/kategorie/dc-netzgeraete/produkt/p-6035.html, visited 08.29.15.

[15] LeCroy, *WaveJet 300A series Oscilloscopes Getting Started Manual*, Apr. 2009. Available online http://cdn.teledynelecroy.com/files/manuals/wj300a-gsm_reva.pdf, visited 08.29.15.

[16] HP, *Website with copy of the datasheet.* http://www.testequipmentdepot.com/usedequipment/pdf/8082A.pdf, visited 09.08.15.

[17] Lumitronix, *Lumitronix website.* http://www.leds.de/Low-Mid-Power-LEDs/LEDs-5mm/Farbige-LEDs/5mm-LED-UV-400mcd-13-3-1V.html, visited 09.07.15.

[18] Arduino, *Arduino Uno product website.* https://www.arduino.cc/en/Main/ArduinoBoardUno, visited 09.08.15.

[19] Atmel, *Datasheet of 8-bit AVR micro-controllers*, 2009. Available online http://www.atmel.com/Images/doc8161.pdf, visited 08.29.15.

[20] Arduino, *Arduino language reference website.* https://www.arduino.cc/en/Reference/AnalogRead, visited 09.08.15.

[21] Texas Instruments, *Datasheet of LMT87, LMT87-Q1*, May 2014. Available online http://www.ti.com/lit/ds/symlink/lmt87.pdf, visited 08.29.15.

[22] Agilent Technologies, *Agilent U1230 Series Data Sheet*, Oct. 2013. Available online http://cp.literature.agilent.com/litweb/pdf/5990-7550EN.pdf, visited 08.29.15.

[23] Voltcraft, *Operating manual of linear switching power supplies.* Available online http://www2.produktinfo.conrad.com/datenblaetter/500000-524999/513020-an-01-ml-Schaltnetzteil_DPS_2010PFC_de_en.pdf, visited 08.29.15.

[24] M. Lauscher, *Characterisation Studies of Silicon Photomultipliers for the Detection of Fluorescence Light from Extensive Air Showers*, master's thesis, III. Phys. Inst. A, RWTH Aachen University, Jan. 2012.

[25] M. Stephan, *Measurement of the Light Flux of Stars and the Night-Sky with Silicon Photomultipliers*, PhD thesis, III. Phys. Inst. A, RWTH Aachen University, Dec. 2014.

[26] A. Biland *et al.*, *Calibration and performance of the photon sensor response of FACT - the first G-APD Cherenkov telescope*, 2014 JINST 9 P10012. Available online http://iopscience.iop.org/article/10.1088/1748-0221/9/10/

P10012/meta;jsessionid=353D0A77DFD4FE223AFF602ECA1D3B9D.c1, visited 07.22.2015.

[27] SensL, *J-Series Datasheet Rev. 1.7, Preliminary*, Aug. 2015.

[28] J. Rosado and S. Hidalgo, *Characterization and modeling of crosstalk and afterpulsing in Hamamatsu silicon photomultipliers*, arXiv:1509.02286v1 [physics.ins-det]. Available online http://lib-arxiv-008.serverfarm.cornell.edu/abs/1509.02286, visited 09.09.2015.

# Acknowledgements
# Danksagungen

An dieser Stelle möchte ich mich bei allen bedanken, die zur Überwindung all der kleinen und großen Herausforderungen dieser Arbeit beigetragen haben.

Zunächst gebührt mein Dank Herrn Prof. Dr. Bretz, der sich stets Zeit zur Beantwortung meiner Fragen nahm und es mir überhaupt erst ermöglichte, meine Bachelorarbeit an seinem Institut zu verfassen.
Mein Dank gilt ebenso Herrn Prof. Dr. Hebbeker, der mich herzlich an seinem Institut willkommen hieß und sich sofort bereit erklärte, die Zweitkorrektur meiner Bachelorarbeit zu übernehmen.

Bedanken möchte ich mich auch bei der gesamten Auger Arbeitsgruppe, die mich herzlich aufnahm und mir einen Einblick in die Arbeitsweise eines Physikers gewährte. Genauso danke ich unserer Sekretärin Adriana Del Piero, die die Bürokratie zu einer herzlichen Angelegenheit machte.
Ganz besonders danke ich meinen Betreuern Johannes Schumacher und Tim Niggemann. Tim half mir bei der Einarbeitung und unterstützte mich bei Herausforderungen von Python sowie der Erarbeitung des Algorithmus. Johannes half mir bei Problemen und Erweiterungen des Messaufbaus weiter und seine Erklärungen und Ratschläge waren besonders in der letzten Phase dieser Arbeit Gold wert. Selbst außerhalb der Arbeitszeiten konnte ich immer mit einer schnellen und kompetenten Antwort rechnen. Daher möchte ich euch erneut herzlich danken.
Ich danke ebenfalls Lukas Middendorf, der mir diverse Fragen beantwortete und sich stets Zeit nahm, wenn es ein Problem mit meinem Aufbau gab, insbesondere als Johannes nicht am Institut war.
Dank meiner Bürokollegen Christine Peters und Markus Lauscher war die Atmosphäre immer heiter. Markus danke ich für die Diskussion unzähliger Detailfragen und Christine gebührt ein besonderer Dank für das ausführliche Korrekturlesen meiner Arbeit.
Auch bedanke ich mich bei Rebecca Meißner, die stets ein offenes Ohr für mich hatte.

Danken möchte ich zudem Fabian, Martin und Tim, mit denen ich durch die Höhen und Tiefen des Bachelorstudiums gewandert bin.
Meinen Eltern danke ich von ganzem Herzen, sie haben mir dieses Studium ermöglicht und mir durch ihren Zuspruch den Weg durch die zahllosen Herausforderungen geleitet. Sie sind ein fester Anker in meinem Leben.
Zu guter Letzt danke ich auch meiner Freundin, Elly, von ganzem Herzen, weil sie immer für mich da ist und mich unterstützt.

# Erklärung

Hiermit versichere ich, dass ich diese Arbeit einschließlich beigefügter Zeichnungen, Darstellungen und Tabellen selbstständig angefertigt und keine anderen als die angegebenen Hilfsmittel und Quellen verwendet habe. Alle Stellen, die dem Wortlaut oder dem Sinn nach anderen Werken entnommen sind, habe ich in jedem einzelnen Fall unter genauer Angabe der Quelle deutlich als Entlehnung kenntlich gemacht.

Aachen, den 16. September 2015

Jan Paul Bernd Koschinsky